Marine and Petroleum Geology 119 (2020) 104448

Contents lists available at ScienceDirect

Marine and Petroleum Geology

journal homepage: www.elsevier.com/locate/marpetgeo

Research paper

Compaction, rock physics and rock properties of sandstones of the Stø Formation: Case study of five wells from the south-western Barents Sea, Norway

Oluwakemi Yetunde Ogebule[a,*], Jens Jahren[a], Nazmul Haque Mondol[a,b]

[a] Department of Geosciences, University of Oslo, P.O. Box 1047, Blindern, 0316, Oslo, Norway
[b] Norwegian Geotechnical Institute (NGI), P.O. Box 3930, Ullevaal Stadion, 0806, Oslo, Norway

ARTICLE INFO

Keywords:
Barents sea
Compaction
Exhumation
Intergranular volume (IGV)
Rock physics
Permeability
Porosity
Velocity

ABSTRACT

Five wells containing Lower-Middle Jurassic sandstones of Stø Formation from the Hammerfest Basin (7120/9–1, 7121/7–1), the Ringvassøy-Loppa Fault Complex (7119/12–1, 7119/12–4) and the Troms-Finnmark Fault Complex (7019/1-1) in the Barents Sea area are considered in this study. The Stø Formation sandstones contain dominantly very fine-to medium-grained quartz arenites with occasional coarse-grained sandstone layers. Feldspathic and quartz wackes are also present. The effect of compaction and exhumation on reservoir properties (porosity and permeability) and seismic property (P-wave velocity) of these sandstones have been investigated. Source of quartz cement has also been investigated. Forty polished thin sections embedded in blue epoxy were studied using optical microscopy, scanning electron microscopy and cathodoluminiscence. Bulk mineralogy was also analysed using X-ray diffraction.

The studied sandstones have experienced Cenozoic exhumation ranging between 820 and 1050 m. P-wave velocity is higher; porosities and permeabilities are lower in the western wells (7019/1-1, 7119/12–1 and 7119/12–4) compared to the eastern wells (7120/9–1 and 7121/7–1). Rock physics models and diagnostics show that the western wells are diagenetically more mature, stiffer, more compacted and more cemented than the eastern wells. These trends are attributed largely to difference in burial history from the east to the west and less to textural variations. Quartz cement is the most important authigenic mineral in these sandstones. Quartz cement in the western well (7119/12–1) is predominantly derived from clay-induced dissolution at macrostylolites whereas the eastern wells (7120/9–1 and 7121/7–1) are mostly sourced from clay-induced dissolution at grain contacts or microstylolites. While cementational porosity loss dominates in the western wells, compactional porosity loss dominates in the eastern wells. Compaction can reduce porosities down to 26% and this might be the reason for better porosity preservation and reservoir quality in the eastern wells than in the western wells.

1. Introduction

The Norwegian Barents Sea area is a highly prospective hydrocarbon province. The Lower-Middle Jurassic Stø Formation is the most important reservoir rock in the area of study. This reservoir rock like every other rock has experienced its properties change continuously from deposition through burial and during uplift. These changes are referred to as compaction.

Compaction is a term that describes porosity reduction and increased density and velocity during burial (Storvoll and Brevik, 2008). Compaction could either be mechanical where changes occur as a function of effective stress or chemical where changes are due to temperature and time (Bjørlykke, 2006). At shallow burial depth, porosity loss is mainly mechanical in siliciclastic rocks and is due to grain reorientation, pseudo-plastic deformation of ductile grains and brittle grain fracturing (Bjørlykke et al., 1989; Bjørkum et al., 1998; Chuhan et al., 2002; Mondol et al., 2007; Fawad et al., 2011). At depositional surface, an intergranular volume (IGV) of about 40% is present in well sorted sands. At the onset of chemical compaction, IGV in sandstones usually vary between 25% and 30% and could be higher in well sorted quartz-rich sands (Rittenhouse, 1971; Houseknecht, 1987, 1988; Stone and Siever, 1996; Ramm, 1992; Paxton et al., 2002; Chuhan et al., 2003).

At deeper burial, porosity loss is chemical in nature. Chemical compaction includes processes that involve dissolution of less stable minerals and precipitation of more thermodynamically stable minerals

* Corresponding author.
E-mail address: o.y.ogebule@geo.uio.no (O.Y. Ogebule).

https://doi.org/10.1016/j.marpetgeo.2020.104448
Received 4 January 2017; Received in revised form 6 April 2020; Accepted 7 May 2020
Available online 11 May 2020

such as smectite transformation to illite and quartz cement at temperatures greater than 70 ^{O}C.

Quartz cement is an important cement in sandstones and this cement is suggested to be sourced from pressure solution (Heald, 1955; Rittenhouse, 1971; Houseknecht, 1984, 1988; James et al., 1986; Stone and Siever, 1996). Pressure solution is a process by which detrital grains or authigenic minerals dissolve at grain-to-grain or intercrystalline contacts (Bjørkum, 1996; Tada and Siever, 1989). What is considered as pressure solution has been argued to be clay induced dissolution-CID (Oelkers et al., 1992, 1996; Walderhaug, 1994; 1996; Bjørkum, 1996; Bjørkum et al., 1998; Walderhaug and Bjørkum, 2003; Walderhaug et al., 2004). Clay induced dissolution involves dissolution of quartz at quartz grain contacts bearing mica or clay either on micro scale (microstylolites) or at high-amplitude stylolites (macrostylolites) through thermodynamic forces rather than stress. The dissolved silica is afterwards diffused a short distance away to other quartz grain surfaces from clay or mica surfaces and precipitates as quartz overgrowths. Dissolution is initiated when there is an increase in the solubility of quartz grains either at grain contacts or along stylolites and solubility increases when the quartz grain is fractured (Bjørlykke and Egeberg, 1993). CID at grain contact is an agent of intergranular compaction which leads to a reduction in IGV but may or may not always lead to reprecipitation of cement in same sample (Rittenhouse, 1971; Tada and Siever, 1989; Bjørlykke et al., 1992; Stone and Siever, 1996). If reprecipitated, quartz cement in this case may cause a reduction in pore volume and an increase in rock (Bjørkum et al., 1998; Bjørlykke, 1998; Thyberg and Jahren, 2011; Walderhaug, 1996).

Quartz cementation process is controlled by precipitation rate (Walderhaug et al., 2004) and will progress further as long as temperatures are greater than 70 ^{O}C and there is availability of pore space to contain such cement. This will continue even during basin uplift or inversion as long as the temperature remains greater than 70 ^{O}C (Bjørlykke and Jahren, 2010).

Previous studies of Upper Jurassic sandstones of the Norwegian Continental Shelf show that reservoir quality and quartz cementation are controlled by thermal exposure variations and grain coating microquartz (Aase et al., 1996; Maast et al., 2011; Ramm et al., 1997). Coatings on sand grains such as chlorite and hematite may retard or disturb quartz overgrowth (Maast et al., 2011). High geothermal gradients combined with low rates of subsidence will cause an increase in rate of quartz cementation or an integrated increase in quartz cement over the same time interval (Walderhaug, 1994, 1996; Walderhaug et al., 2004).

Compaction processes in sedimentary basins influence seismic properties such as velocity and bulk density (Marcussen et al., 2010). The interplay between sandstone reservoir parameters including grain size, sorting, shape, porosity, number of grain contacts, and clay contents strongly control compaction behaviour in sandstones (Zadeh et al., 2016; Fawad et al., 2011; Giles, 1997; Bjørlykke et al., 2004; Waples and Couples, 1998). Grain size and grain strength play significant roles in mechanical compaction. Well sorted coarse-grained sand has a higher compressibility than fine-grained sand when the mineralogy is the same. Shaly sandstones have lower porosity which in turn causes higher velocities than in quartz-rich sandstones. On the otherhand, Quartz-rich sandstones have higher velocities than shaly sandstones for the same porosity as a result of mineralogy effect (Chuhan et al., 2002, 2003; Fawad et al., 2011; Zadeh et al., 2016). Differences between experimental mechanical compaction of shales (Mondol et al., 2007), sands (Fawad et al., 2011; Zadeh et al., 2016), and well log data may be attributed to exhumation, overpressure, cementation, or hydrocarbon emplacement (Storvoll et al., 2005). The differences between compaction trends and well logs and the gap between seismic properties and reservoir properties are bridged and better understood through rock physics (Avseth et al., 2010a, 2010b).

Rock physics models are used to diagnose rock texture of shales and sandstones when velocity and porosity are known. Dræge (2011) for example came up with a diagenetic rock physics model that incorporated temperature in its modelling of sandstones and shales. Local geologic trends including compactional and depositional trends are used to constrain rock physics models. The slope of velocity-porosity trends in sandstones is largely controlled by the geologic process that defines porosity (Dvorkin and Nur, 1996; Vernik and Nur, 1992; Han et al., 1986). Steep velocity-porosity trends in sandstones are attributed to diagenetic effects such as compaction, cementation and pressure solution on porosity hence, such steep velocity-porosity trend is referred to as compactional trend, whereas, depositional trends which are controlled by sorting and clay content yield flatter velocity-porosity trends. Rock physics models such as contact cement model of Dvorkin and Nur (1996), constant cement model of Avseth et al. (2000) and modified upper Hashin Shtrikman bounds (Hashin and Shtrikman, 1963; Berryman, 1995) are some models that easily diagnose cementation in rocks. Rock physics template (RPT) was first introduced by Ødegaard and Avseth (2003). RPT is a locally constrained chart that models lithology and fluid prediction through a combination of diagenetic and depositional trend with Gassmann fluid substitution.

The Barents Sea is a complex area which has experienced several episodes of rifting, subsidence, upliftment, erosion, and reburial. A combination of uplift and erosion is referred here as exhumation. Various studies on the estimation of exhumation in the Barents Sea area have been done (e.g. Baig et al., 2016; Dimakis et al., 1998; Henriksen et al., 2011; Nyland et al., 1992; Ohm et al., 2008; Riis and Fjeldskaar, 1992; Storvoll et al., 2005). Exhumation plays an important role in defining present day properties of rocks including reservoir, source, and cap rocks.

Bjørlykke et al. (1989) stressed the importance of reconstructing the burial and uplift history for compaction studies as compaction of sedimentary rocks are strongly dependent on mineralogy, burial history and temperature. Exhumation estimates have been obtained through different techniques by several workers including Baig et al. (2016), Henriksen et al. (2011), Ohm et al. (2008), Storvoll et al. (2005), Hansen (1996), and Densley et al. (2000). Various established techniques for carrying out exhumation estimation are also discussed by Magara (1978). Magara (1978) discussed the preference of shale velocities over sandstones for exhumation studies. Velocity data are useful for the analysis of sedimentary basins as tools for lithology, facies, fluid and overpressure recognition as well as for burial and temperature history reconstruction (Storvoll et al., 2005). In uplifted areas, there is a shift in the normal compaction trend of shales in a direction of increased compaction when compared to an area which is not uplifted.

The changes in porosity and permeability might not follow a well-defined trend in sedimentary basins as they are controlled by environmental variations and depositional processes (Bjørlykke, 1988; Ali et al., 2010). It is therefore important to understand porosity and permeability distribution in sandstones within the context of its own sedimentary basin. This is accomplished by understanding the processes that may preserve or destroy porosity and permeability within such a basin (Bjørlykke, 1988).

An understanding of how exhumation may affect compaction, diagenesis and reservoir properties has been a strong motivation for this study. This research therefore aims to understand the behaviour of reservoir rock properties such as velocity, porosity and permeability with respect to compaction and exhumation of sandstones. In addition, the study aims to investigate controls on reservoir quality, to understand porosity preservation mechanism in the chemical compaction domain and finally, to understand the source of the quartz cement.

The present study focuses on the Jurassic sandstones of the Stø Formation in five wells from the Norwegian Barents Sea. Summary information on the wells is shown in Table 1. These sandstones have been evaluated by an integrated approach which is categorized into two parts. Part 1 contains petrophysics and rock physics analyses from well logs. Compaction, exhumation estimation and correction were done on mudrocks. For the sandstones, brine substitution was carried out and in

Table 1
General information of studied wells.

	7019/1-1	7119/12-1	7119/12-4	7120/9-1	7121/7-1
Kelly bushing (m)	24	25	23	23	22
Water depth (m RKB)	190	200	192	320	329
Total depth (MD-mRKB)	3003	3088	2917	2300	2160
Final vertical depth (m RKB)	2998	3087	2910	2300	2160
Bottom hole temperature (°C)	108	96	105	73	72
Bottom hole temperature (°C) before exhumed	138	124	138	109	110
Paleo-temperature at Top of Sto Formation (°C)	117	110	115	93	99
Geothermal gradient (°C/Km)	37	32	37	35	37
Maximum burial depth of Top Sto Formation (m RKB)	3266	3533	3196	2889	2898

turn used in the evaluation of rock physics depth trends and rock physics diagnostics. In situ rock properties were used for rock physics template.

Part 2 shows core and thin section evaluation. We make use of optical microscopy on thin sections for point counting of minerals and pore space; grain size analyses of 50 grains per thin section and sorting estimation of the sandstone grains. Scanning electron microscopy has also been implemented for cementation and mineralogy analyses on stubs and in thin sections. In addition, X-ray diffraction is used to analyse for both bulk and clay mineralogy of the sandstones. Data on helium porosity and permeability are obtained from the Norwegian Petroleum Directorate website. A summary of the workflow utilized in our study is presented in appendix and is further discussed in section 3-Materials and Methods. The data generated in this study may be useful for rock physics modelling in the chemical compaction zone. The data is also applicable to quartz cementation modelling in order to better understand the timing of cementation and the overall effect of cementation on basin history. This in turn can be useful to improve the interpretation of well log and seismic data.

2. Geological background and structural setting

The study area generally lies within the south-western Barents Sea and includes parts of the Snøhvit Field of the Hammerfest Basin; the Ringvassøy-Loppa Fault Complex which borders the Tromsø Basin and the Hammerfest Basin; and the Troms-Finnmark Fault Complex adjacent to the Tromsø Basin (Fig. 1a and b). The Hammerfest Basin which is host to wells 7120/9–1 and 7121/7–1 trends ENE-WSW. It is a relatively shallow basin which divides into western and eastern sub-basins. The western sub-basin, which contains some wells of interest in this study, dips westwards towards the Tromsø Basin and contains fault systems that trend E-W, ENE-WSW and WNW-ESE. The basin dates back to Late Devonian-Early Carboniferous and contains Upper Paleozoic to Cenozoic sediments. The eastern sub-basin is less faulted (Berglund et al., 1986; Gabrielsen et al., 1990; Linjordet and Olsen, 1992). Faults were reactivated in the Late Jurassic to Early Cretaceous. Ringvassøy-Loppa Fault Complex (RLFC) houses well 7119/12–1 and well 7119/12–4. RLFC was first defined by Gabrielsen et al. (1984) as a north-south trending area with west-dipping major faults. RLFC is a zone of transition from the Tromsø Basin to the Hammerfest Basin and it meets the Troms Finnmark Fault complex to the south (Fig. 1b). The main subsidence in this area was initiated in Mid-Jurassic and reached its peak in the Early Cretaceous. Fault reactivation took place in the Late Cretaceous which further affected the Tertiary strata in the area (Gabrielsen et al., 1990). Troms-Finnmark Fault Complex which hosts well 7019/1-1 is a north-east trending boundary (Fig. 1a) between more stable southern and south-eastern landward platform areas and basinal areas of Upper Paleozoic to Cenozoic age such as the Tromsø Basin and the Hammerfest Basin (Gabrielsen et al., 1990; Olaussen et al., 1984). This zone consists of normal faults which date back to Pre-Permian, but these faults were reactivated episodically from the Late Cretaceous to Early Tertiary up until the Eocene. Maximum subsidence/burial along the fault complex is in the Late Jurassic to Early Cretaceous (Gabrielsen et al., 1990).

Rifting was initiated in the SW Barents Sea in the Middle-Late Jurassic as indicated by the Middle-Late Jurassic sequence boundary shales/mudstones (Faleide et al., 1993). The Jurassic stratigraphy of the south-western Barents Sea is divided into two distinct Groups which are Kapp Toscana and Adventdalen groups (Fig. 2). These two Groups are separated by a rifting event which defines the paleo-environment of deposition for each group. The Kapp Toscana Group is of pre- and syn-rift and is exposed to deltaic and shallow marine environment which largely contains sandstones. The main reservoirs in the South Western Barents Sea are these Kapp Toscana sandstones to which the Stø Formation belongs. The Adventdalen Group is of post-rift period and deep sea environment which comprises of mudrocks that bear the source rocks (Fuglen and Hekkingen formations) of the area.

In the Early Jurassic, global sea level began to rise causing the deposition of the Stø Formation in a shoreline and near shore depositional environment where bioturbation and storm-wave processes prevailed (Olaussen et al., 1984). The upper part of the Stø Formation represents more distal marine facies i.e. lower shoreface to offshore environments. Fine to medium grained sandstones dominate the Stø Formation over a large area. The lower unit of the Stø Formation (S-I in Fig. 2) suggested by Olaussen et al. (1984) consists of moderately sorted fine-grained sandstones interlayered with well sorted sandstones. It is occasionally bioturbated and contains silty laminations. More rounded coarse-grained sandstones occur and these are described as storm generated beds (Olaussen et al., 1984) but due to the presence of intra-formational mudclasts, Ramm (1991) describes it as indicative of channel fill deposits. The middle unit of the Stø Formation (S-II in Fig. 2) contains clayey laminations and is bioturbated occasionally with pyrite present which is indicative of an offshore environment. High siderite content however indicates a possible lagoonal or isolated bay environment with periodic freshwater or brackish water influx (Ramm, 1991). The uppermost unit of the Stø Formation (S-III in Fig. 2) dominantly contains fine-grained, moderate to well sorted sandstones of high energy beach or bar environment (Olaussen et al., 1984; Ramm, 1991).

Most pertinent to this study are the Cenozoic uplift and erosion episodes that have strongly influenced the most parts of the Barents Sea and have led to present burial depths that differs from the maximum burial depths the rocks might have experienced. These episodes of uplift and erosion are depicted as two regional unconformities including the base Paleogene unconformity and the Upper Regional Unconformities. (Baig et al., 2016; Faleide et al., 1993).

3. Materials and methods

This study is comprised of two sections and the materials and methods for each section is summarized in the appendix. The first part contains petrophysical observations and analyses. Well logs from five studied wells (7019/1-1, 7119/12–1, 7119/12–4, 7120/9–1 and 7121/7–1) were first corrected for uplift using shales and mudrocks. A study of petrophysical properties of Stø reservoir sandstones for the five wells

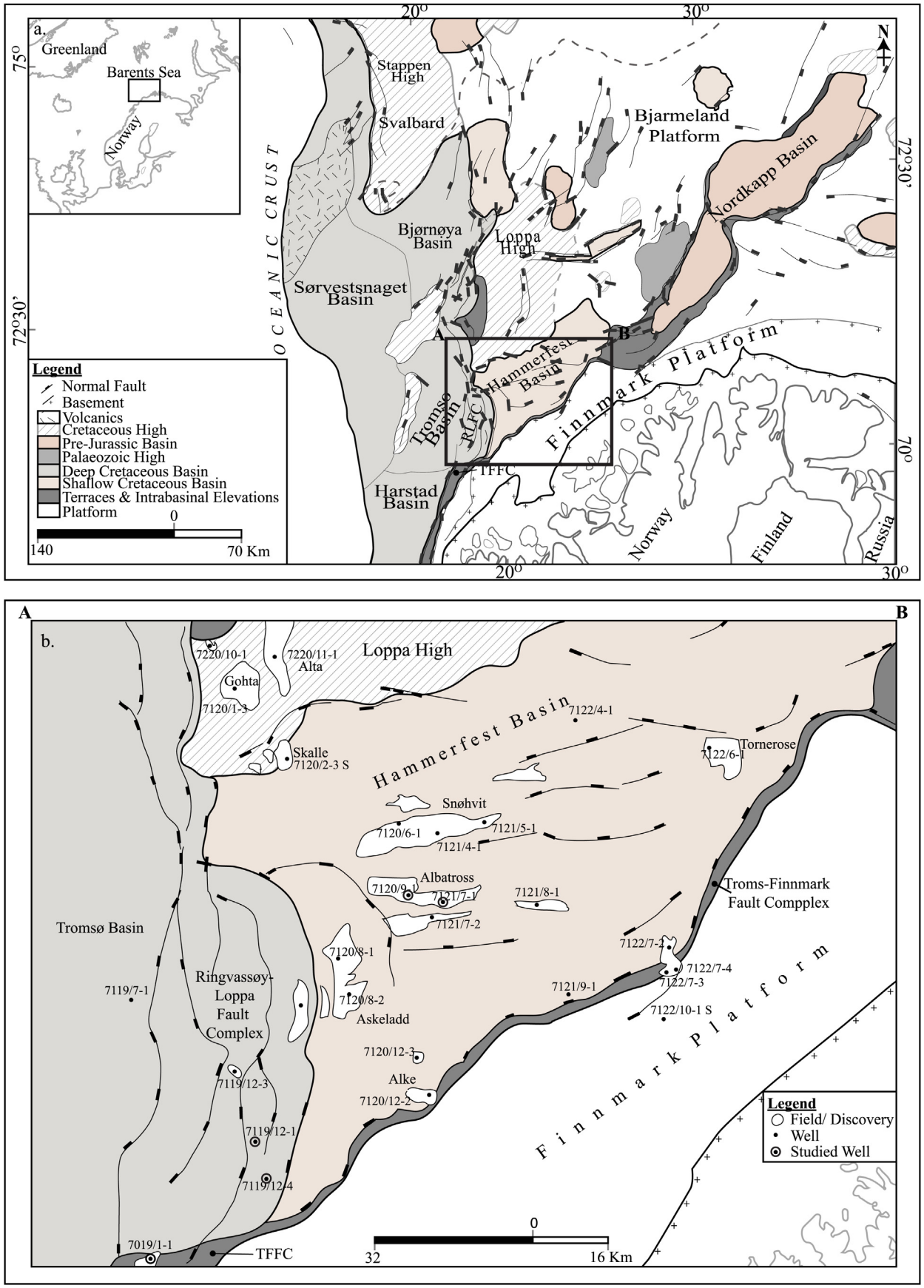

Fig. 1. a) Regional map and b) Geological map of the study area showing well locations, main structural features, geological boundaries, hydrocarbon fields and discoveries. TFFC = Troms-Finnmark Fault Complex. The maps are modified from Nooraiepour et al. (2017) and NPD (2019).

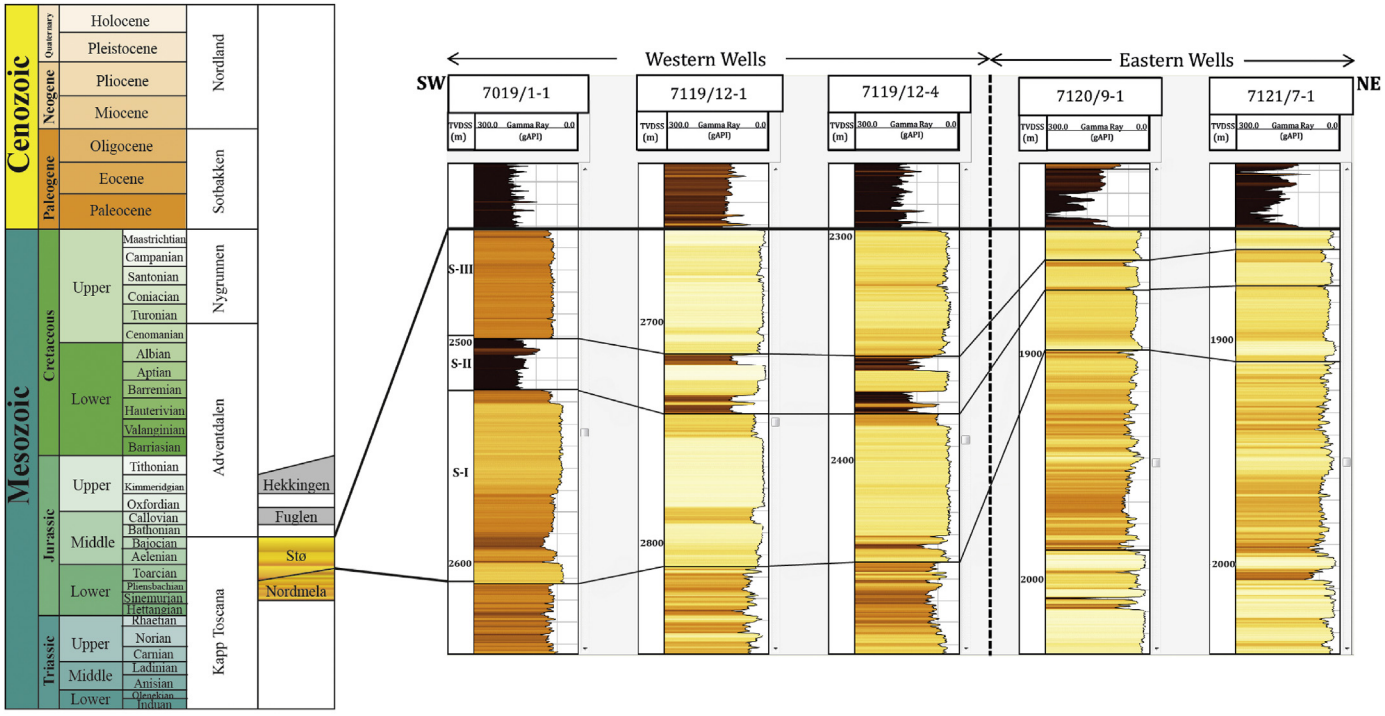

Fig. 2. Lithostratigraphic correlation of the Stø Formation using gamma ray logs. The gamma-ray log is reversed so that it gives a semblance to a sedimentary log. Colour variation in the units is based on shale volume. The Geological Time Scale and stratigraphic succession are modified from Glørstad-Clark et al. (2010). (For interpretation of the references to colour in this figure legend, the reader is referred to the Web version of this article.)

was also carried out. Log types used include gamma-ray, compressional wave transit time (P-wave), bulk density, neutron and resistivity logs. Shear wave transit time was available only in well 7119/12–4 while it was calculated for other wells using Shear Sonic QC/Create module after Greenberg and Castagna (1992) in Interactive Petrophysics (IP). Gamma Ray Index (Z) was computed for each well from equation **(1)** (Asquith et al., 2004). Corresponding shale volumes were calculated for Tertiary rocks and older than Tertiary clastics after Larionov (1969) as shown in equations **(2)** and **(3)** respectively.

$$Z = (Gr - Gr_{Clean}) / (Gr_{Clay} - Gr_{Clean}) \quad (1)$$

$$Vsh = 0.083\ (2^{3.7Z} - 1) \quad (2)$$

$$Vsh = 0.33\ (2^{2Z} - 1) \quad (3)$$

Where Z is the Gamma Ray Index, Vsh is the Gamma Ray-computed shale volumes, Gr is the gamma ray value from the log, Gr_{Clean} is the gamma ray value in the cleanest sandy zone and Gr_{Clay} is the gamma ray value for the most clay-rich zone. In addition to this, for the sandstone sections, a resistivity and a neutron-density approach to clay volume computation were done interactively within the IP software. An average from the gamma ray, neutron-density and resistivity calculated shale volumes were then applied in such zones. This corrects for the presence of hydrocarbon in the sandstones. Carbonate layers were excluded by the use of neutron-density cross plot.

As the Stø Formation is pre-Tertiary in age, a shale volume cut off of 0.25 from equation **(3)** is used to discriminate sandstones from other lithologies in this study. Lithostratigraphic correlation across the five wells is carried out by the use of reversed Gamma Ray logs, colour-coded by clay volume (Fig. 2). These reversed plots were made to mimic sedimentary logs. In Fig. 2, the wells are grouped into western and eastern wells; the western wells include wells 7019/1-1, 7119/12–1 and 7119/12–4 while the eastern wells include wells 7120/9–1 and 7121/7–1. The three Stø Units S- I, S-II and S-III are shown in the correlation panel in Fig. 2.

Exhumation estimation was carried out using compressional velocity data of mudrocks (Vsh > 0.75) and experimental curves of Mondol et al. (2007). In order to calculate exhumation, velocity-depth trends in shallow mudrocks of the five wells were compared to empirical velocity depth trends of Mondol et al. (2007). Data were plotted at 5m intervals for the mudrocks and estimate of exhumation was obtained by shifting the log data points downward in depth until it closely matched the empirical trends (Fig. 3) and such change in depth was measured as an estimate of exhumation. Experimental curves of Mondol et al. (2007) are limited in their use as they do not take chemical compaction into account and might be best suited to uncemented lithologies of known mineralogy.Values obtained from this procedure are included in Table 2 along with values extracted from published maps and papers including Baig et al. (2016), Ohm et al. (2008), Storvoll et al. (2005), Henriksen et al. (2011), and Mondol et al. (2007). Exhumation estimate (see Table 2) from Baig et al. (2016) was the preferred choice because the estimation involved the use of several methods and data rather than an assumption of mineralogy to match an experimental curve as was done above. Estimates from Baig et al. (2016) were added to the present burial depth to give the possible maximum burial depth for the rocks. The total depth and bottom hole temperature available (Table 1) were used to compute for the geothermal gradient which was in turn used along with the maximum burial depth to compute for the maximum temperature the rocks might have been exposed to (see Table 1). A limitation to the use of bottom hole temperatures for estimation of paleotemperatures is that they may differ from true formation temperatures as a result of circulation of drilling mud. Also, the measurements may be uncertain and may be unreliable for older wells. We assumed a linear geothermal gradient but this may not be the case as the uplift may cause steeper temperature gradients at shallower layers than in deeper layers. In addition, present day temperatures as well as geothermal gradients may not necessarily represent the past. Differences in paleo-geothermal gradients from the present ones will affect exhumation estimates. In this study, we therefore assumed for simplicity that the geothermal gradients were constant through time in order to estimate for paleotemperatures.

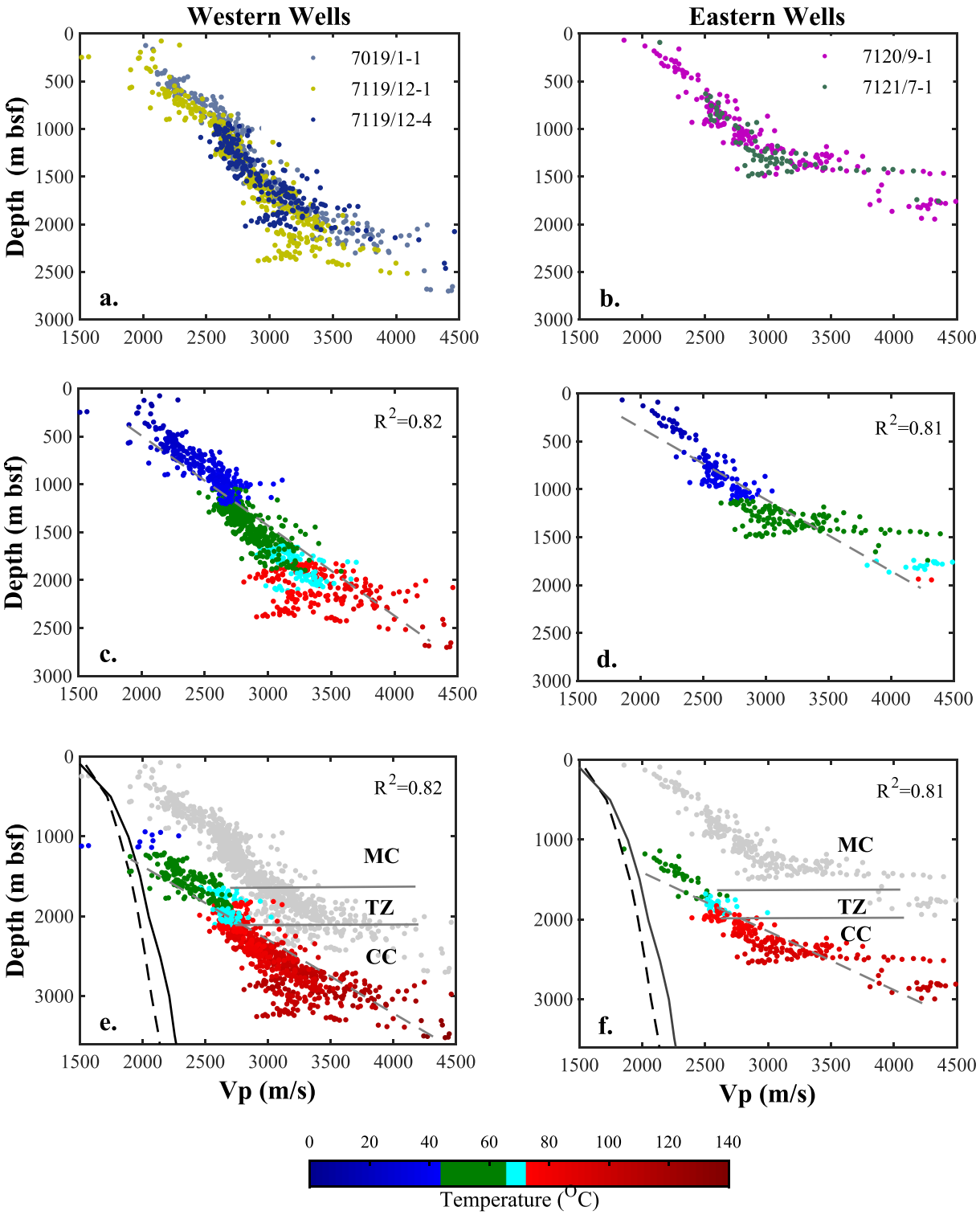

Fig. 3. Velocity-depth trends for mudrocks (Vsh > 0.75) of western wells −7019/1-1, 7119/12–1 and 7119/12–4 (left) and eastern wells −7120/9–1 and 7121/7–1 (right). Figures a and b show velocity at present burial depth, colour-coded by wells; c and d show velocity at present burial depth colour coded by present day temperature. Figures e and f show velocity at present burial depth (gray points) and at maximum burial depth (coloured points colour-coded by the maximum temperature experienced before uplift). Dashed line is experimentally compacted 80:20 smectite-kaolinite curve while the solid line is 60:40 smectite-kaolinite curve from Mondol et al. (2007). MC, TZ and CC are mechanical compaction, transition zone and chemical compaction respectively. (For interpretation of the references to colour in this figure legend, the reader is referred to the Web version of this article.)

Rock physics diagnostics of the sandstones were carried out on velocity-porosity trends for brine-saturated sandstones along with overlain rock physics models and elastic bounds while rock physics templates were used to understudy the original rocks. The sandstones were substituted with brine using fluid substitution module in IP (Gassmann, 1951; Avseth et al., 2010a, 2010b) and Batzle and Wang (1992) relations. The model lines were created under the assumption that the rock is pure quartz with a depositional porosity of 40%. Rock physics and

Table 2
Exhumation estimates from literature and from experimental compaction curves.

References	Well Names				
	7019/1-1	7119/12-1	7119/12-4	7120/9-1	7121/7-1
Baig et al. (2016)	820	875	900	1050	1050
Ohm et al. (2008)	750	785	900	785	785
Storvoll et al. (2005)	–	900	–	–	–
Henriksen et al. (2011)	–	–	–	1000	1000
Mondol et al. (2007):					
Smectite: Kaolinite (60:40)	1650	750	–	839	777
Smectite: Kaolinite (80:20)	2050	1150	–	1197	1445.2

petrophysical plots were made at 5m intervals for the western wells and at 1m interval for the eastern wells where data points were fewer.

The second section contains core and thin section studies and observations. Forty polished thin sections were available from core samples at selected depths from wells 7119/12–1, 7120/9–1 and 7121/7–1. All samples were impregnated with blue epoxy in order to highlight porosity. These thin sections were studied under an optical microscope and point counted twice with three hundred points per thin section. Average results were taken of each counted parameter including mineralogy, primary (intergranular) porosity and secondary (intragranular) porosity. Grain size was determined by measuring the long axis of fifty grains per thin section and calculating the mean value. Sorting was computed with the aid of GRADISTAT (Blott and Pye, 2001) as standard deviation of the long axis measurement of the fifty grains per sample. The thin sections were also examined with a scanning electron microscope (SEM) for quartz overgrowth, clay coatings on the surface of quartz grains, clay content and estimation of percentage area covered by porosity and minerals for comparison with estimates obtained from thin section counts. Bulk mineralogical composition was analysed through X-ray diffraction (XRD). Twenty two untreated and non-oriented samples from two wells (wells 7120/9–1 and 71217–1) were analysed on a Bruker D8 ADVANCE using CuKα radiations for identification of mineral phases. Semi-quantitative determination of the mineral phases was obtained automatically through DIFFRAC.EVA. Bulk mineralogy XRD for the well 7119/12–1 was obtained from Ramm (1991) while that of the clay mineralogy was calculated from data obtained from Ramm (1991) by using a method described by Peltonen et al. (2008). Carbonate- and clay-rich sections were excluded as the focus of the study is only on sandstones.

Core reports for three of the wells including wells 7119/12–1, 7120/9–1 and 7121/7–1 were available from the Norwegian Petroleum Directorate. From these, laboratory measurements of porosities and permeabilities were obtained. The modal values of porosities from each Stø Unit were compared to that obtained from point-counting on thin section, from area measurement analysis of samples under the scanning electron microscope (SEM), and from helium porosity in order to satisfactorily determine which of the log-derived porosity models match closely with the core-derived porosity. The porosities estimated from cores seem to match the bulk density derived porosities better. Hence, the bulk-density porosity is used as log-porosities in this study.

4. Results

4.1. Part 1: petrophysics and rock physics analyses

4.1.1. Exhumation and maximum burial depth

Fig. 2 shows the top of the Stø Formation decreases in present depth from the western wells to the eastern wells. A summary of exhumation estimates of the five wells is presented in Table 2. From Table 2, Baig et al. (2016) estimates were selected and used to obtain the maximum burial depths and corresponding maximum temperatures which are included in Table 1. Exhumation is observed to steadily increase from the most western well at about 820m to the eastern wells at up to 1050m. Considering the Stø Formation which is the focus of this study, exhumation corrections suggest that the top of the formations (see Table 1 & Fig. 4a and b) in the western wells are more deeply buried than those of the eastern wells. From Table 1, well 7119/12–1 is the most deeply buried at about 3500m from rotary Kelly bushing (RKB) (~3300m from bottom of sea floor, bsf) followed by wells 7019/1-1, 7119/12–4, 7121/7–1 and the least buried being well 7120/9–1 at a maximum burial depth of about 2900m RKB (~2500m bsf). Maximum burial depth after exhumation correction is deepest in the west and becomes shallower towards the east while the amount of exhumation decreases westward with the eastern wells being the most uplifted and western well 7019/1-1 being the least uplifted.

4.1.2. Velocity – depth trend

Velocity-depth data of all brine-substituted sandstones (Vsh $<$ 0.25) from the five wells are plotted on Fig. 4a to d. The brine substituted sandstones are used here in order to eliminate the influence of different reservoir fluids. The location of the Stø Formation along the wells are shown in Fig. 4a for the western wells and in Fig. 4b for the eastern wells. Fig. 4a and c shows that the western wells have velocities ranging from about 3500 m/s to about 5200 m/s with more data point in the $>$ 4500 m/s range. Also, the wells 7019/1-1 (filled circles) and 7119/12–1 (open circles) have higher velocities than the well (open stars). The sandstones of these wells have undergone maximum temperatures ranging from about 110 ^{O}C to about 130 ^{O}C (Table 1). On the other hand, Fig. 4b and d shows that the eastern wells have velocities ranging from about 3500 m/s to about 4000 m/s with most of the data being less than 4000 m/s and a few data points greater than 4500 m/s. Maximum temperatures experienced by the eastern wells range from over 90 ^{O}C to about 100 ^{O}C (Table 1).

4.1.3. Porosity-depth trend

Porosity-depth trends are plotted in Fig. 4e and f. The western wells 7019/1-1 and 7119/12-1 have porosity ranging from about 2% to 15% with modal porosity values of about 5–8% while well 7119/12-4 has porosity ranging from around 15% to almost 30% (Fig. 4e). In the eastern wells, porosity ranges from about 10 to greater than 25% with a modal porosity value of 15–20% (Fig. 4f). Shale volume which is coloured onto the plots shows a more obvious effect in the well 7121/7–1 (open circles) as higher porosities are observed where the volume of shale is least whereas, lower porosities are seen where shale volume relatively higher.

4.1.4. Porosity – velocity trend

The effect of maximum temperature and shale volume on porosity-velocity (Vp and Vs)) trends are shown for brine-saturated sandstones of the Stø Formation in both the western wells and eastern wells (Fig. 5). Overlain on these plots are rock physics trends including constant cement lines, modified upper Hashin Shtrikman bound, and modified lower Hashin Shtrikman bound (for 0% Cement line or unconsolidated line). A linear inverse dependence of velocity on porosity is observed in these wells with the western wells having much higher velocities and corresponding lower porosities than in the eastern wells. Western wells 7119/12–1 (Fig. 5a, e); 7019/1-1 and 7119/12–4 (Fig. 5c, g) have experienced similar maximum temperatures but a difference is observed in their positions relative to the cement lines. The eastern wells (Fig. 5b, d, f and h) on the other hand have experienced lower temperatures than the western wells and are positioned relatively lower than the western wells.. Well 7119/12-1 have quartz cement dominantly between 1 and 5% with a few sandstones having cements

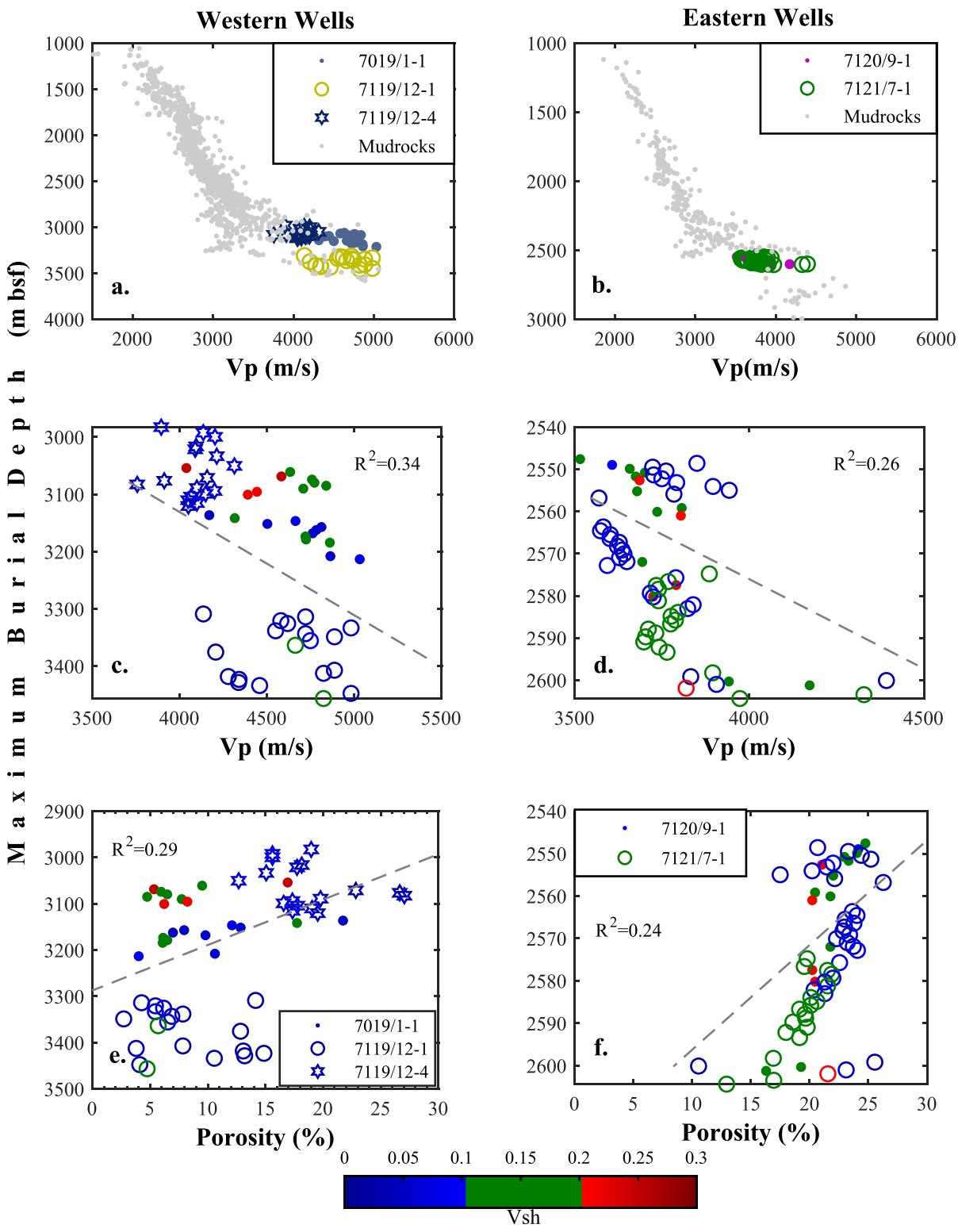

Fig. 4. a) Plot of Vp versus maximum burial depth showing the location of the Stø Formation sandstones (Vsh < 0.25; coloured by well)) relative to the mudrocks (gray dots) of the western wells (7120/9–1, 7119/12–1 and 7119/12–4) and b) the eastern wells (7120/9–1 and 7121/7–1); c) plot of sandstones of the Stø Formation of the western wells and d) of the eastern wells; e) plot of porosity versus maximum burial depth of the Stø Formation sandstones in the western wells and f) in the eastern wells.

between 5 and 10% (Fig. 5a,e). Well 7019/1-1 have few of the sandstones plotting between 1 and 5% quartz cement line while most plot between 5 and 10% (Fig. 5c,g). Well 7119/12-4 plots predominantly between the 10 and 15% quartz cement lines with three points plotting on scheme 2-modified upper Hashin Shtrikman line on the Vs-Porosity plot (Fig. 5g). This might be an indication of the presence of some grain-to-grain contact cements in these three samples. The eastern wells 7120/9–1 and 7121/7-1 plot are have cements between 5 and 10% (Fig. 5b, d, f, h).

A plot of all five wells and overlays of Voigt upper bound and Reuss

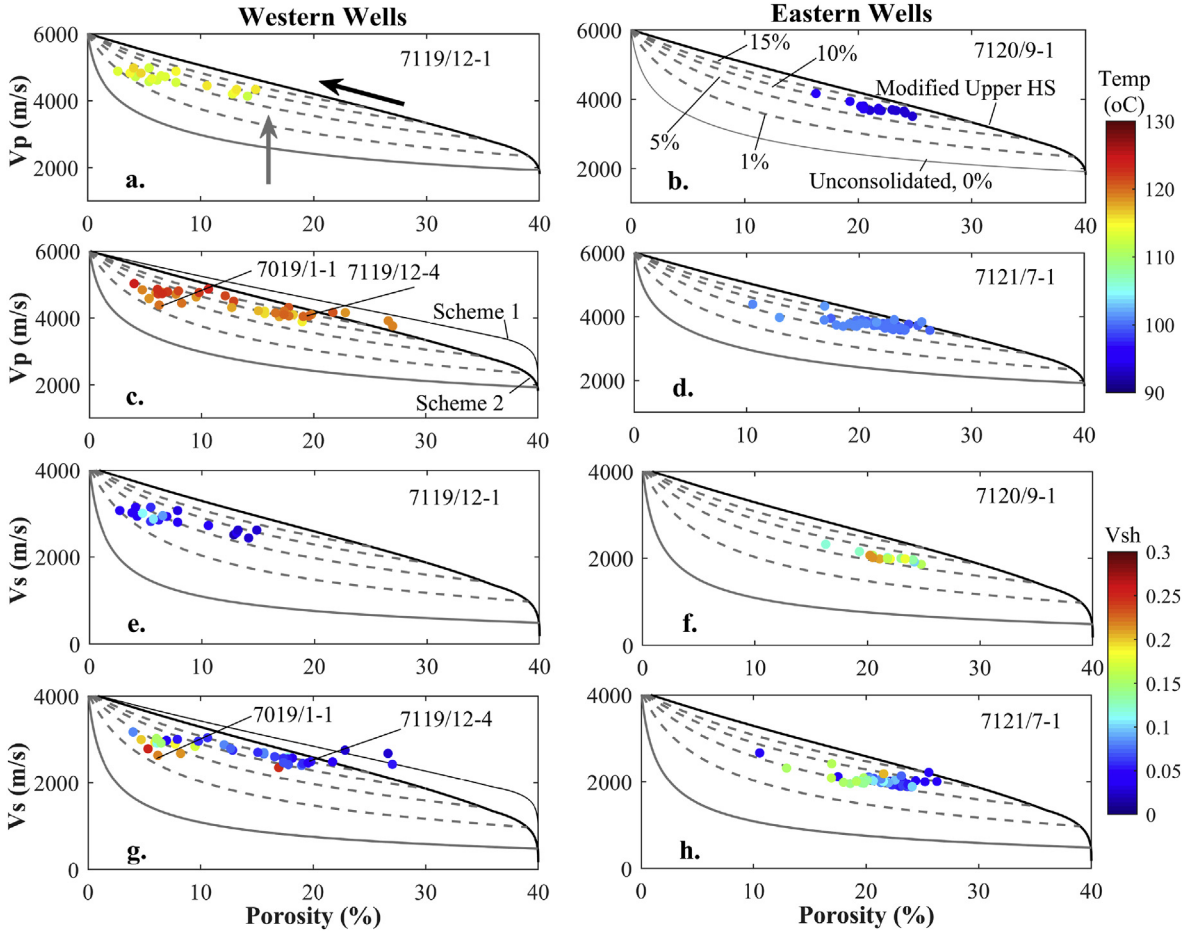

Fig. 5. Rock physics plots of porosity versus velocity overlain with modified upper Hashin-Shtrikman bound, contact cement, and different constant cement lines for western wells (left) and eastern wells (right). Figures a, b, c and d are plots of porosity versus Vp colour-coded by maximum temperaturewhile figures e, f, g and h are corresponding Vs plotscolour-coded by shale volume. Black diagonal arrow indicates increasing diagenetic trend while gray arrow shows increasing depositional trend or increasing burial depth or age. (For interpretation of the references to colour in this figure legend, the reader is referred to the Web version of this article.)

lower bound (Fig. 6a, c) further depicts the difference in relative positioning of these wells on velocity-porosity plots with an increase in velocity and decrease in porosity trending from the eastern wells to the western wells.

4.1.5. Acoustic impedance – Vp/Vs ratio

Fig. 7 represents a plot of acoustic impedance versus Vp/Vs ratio of select wells with Vs predicted for all wells except well 7119/12–4. The sandstones are plotted here with their in-situ fluids with no fluid substitution carried out. Fig. 7a represents the high velocity – low porosity western well 7119/12–1. This well was modelled with 15% quartz cement. Vp/Vs ranges between approximately 1.6 and 1.7 while acoustic impedance ranges between 10000 and 13000 g/cc*m/s. The oil saturated sandstones are seen to lie along the brine sand line. The intermediate velocity-porosity western well 7119/12–4 is shown in Fig. 7b. This dry well was modelled using 10% quartz cement. The brine saturated sandstones are sitting on or close to the modelled brine sand line with Vp/Vs ratio ranging between 1.65 and less than 1.8 while acoustic impedance varies from 8000 to 10500 g/cc*m/s. The eastern well 7120/9–1 (Fig. 7c) is gas saturated and plots within the gas zone beneath the brine sand line. The well was modelled with 5% quartz cement. Vp/Vs varies between 1.65 and slightly greater than 1.8 while acoustic impedance ranges from 7500 to 10000 g/cc*m/s in this well. The modelling shows that Vp/Vs will increase as acoustic impedance decreases but this is not observed in these wells. Rather, acoustic impedance increases from the western well to the eastern well with similar Vp/Vs in the three wells.

4.2. Part 2: core and thin section observations

As previously mentioned, thin sections from the Stø Formation were available from three of the five wells being studied. A summary of modal analyses from point counting under an optical microscope for all three wells is shown in Tables 3 and 4. This excludes all carbonate- and clay-rich sections in order to account for the general variations in the clean sandstones only. Observations are taken from the eastern well 7119/12–1 of the Ringvassøy-Loppa Fault Complex and the western wells 7120/9–1 and 7121/7–1 of the Hammerfest Basin.

4.2.1. Petrography

Quartz: Quartz (in volumetric-percentage) is present in amounts ranging from 76 to 100% in XRD analysis of well 7119/12–1 (Fig. 8a created from data in Ramm, 1991) while it ranges from 91 to 98% in well 7120/9–1 (Fig. 8c) and from 83 to 99% in well 7121/7–1 (Fig. 8d). The ratio of quartz to clay, feldspar and carbonate minerals present both from XRD analysis and from point counting from thin sections shows that the Stø Formation sandstones are predominantly quartz arenites. This is easily seen in Fig. 9 where the data clusters around the 100% Quartz axis. Quartz wackes and feldspathic wackes are present but less common (Tables 3 and 4). Authigenic quartz overgrowths on monocrystalline quartz grains are prominent in these wells and this is the most important cement volumetrically in the Stø Formation (Tables 3 and 4; Fig. 10a and b). In the western well 7119/12–1, quartz cement ranges in volume from about 1 to 28% (Table 3), while in the eastern wells, it ranges from 5 to 18% in well 7120/9–1 (Table 3) and from 3 to

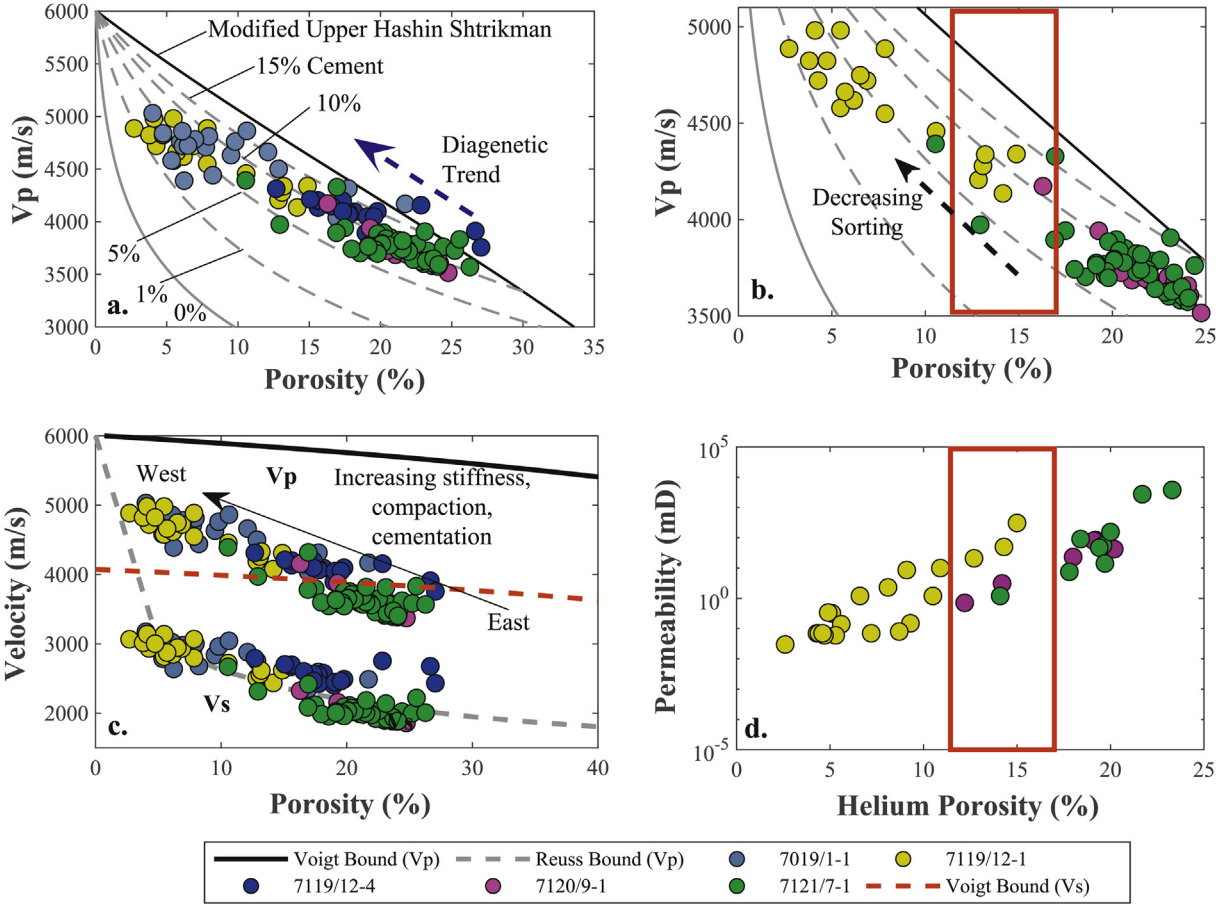

Fig. 6. Porosity versus a) Vp for all five wells overlain with rock physics models. The blue arrow direction indicates increasing diagenetic trend and it is parallel to the modified upper Hashin Shtrikman line. It represents diagenetic trend for more clay-rich sandstones; b) Vp for wells 7119/12–1 and the eastern wells. The broken black arrow shows direction of decreasing sorting c) A plot of porosity versus Vp (top) and Vs (bottom) of all five wells overlain with Voigt upper bound and Reuss lower bound.; d) Helium porosity versus permeability plot. The red box focuses on areas of similar porosity but different permeabilities. See detailed explanation in section 5.2. (For interpretation of the references to colour in this figure legend, the reader is referred to the Web version of this article.)

19% in well 7121/7–1 (Table 4). Amongst the three wells, the western well 7119/12-1 shows a higher amount of quartz cement than the eastern wells with an average of 16.8%. Among the two eastern wells, well 7120/9-1 seems to bear slightly higher amounts of quartz cements (average of 12.1%) than the neighbouring well 7121/7–1 with an average of 10.6%. It should be noted that quartz cement quantification may not be accurate from thin section analysis as the detrital quartz grain is not always separated from the authigenic quartz by dust rim. In addition, under cathodoluminescence, not all quartz grains are illuminated enough to separate and quantify associated quartz cement.

Feldspar: XRD analysis of well 7119/12–1 (Fig. 8a) by Ramm (1991) shows that K-feldspar is almost non-existent or occurs in trace amounts in most part of the Stø Formation. An exception to this is found in lower unit (S-I) at 2785 and 2788.90 m RKB with amounts between 3 and 5%. Plagioclase feldspar occurs in amounts between 1 and 7% in all three units (S-I to S-III) of the Stø Formation in this well 7119/12–1 (Ramm, 1991). In the eastern wells, K-feldspar and plagioclase (Fig. 8c and d) are present in almost equal amount where K-feldspar ranges from about 1 to 1.5% and plagioclase ranges in volume from about 0.2 to 2.1%. Sample distribution of feldspars in sandstones of an eastern well is shown in Fig. 10c and d.

Carbonates: The sections with high carbonate content (such as in Fig. 10e and f) have been excluded from the clean sandstones as this study focusses on sandstones rather than carbonates. In the Stø Formation sandstones, carbonates occur generally in trace amounts (Tables 3 and 4). The western well 7119/12–1 contains authigenic ankerite and siderite (Fig. 8a). Siderite is present in the top section of S-II and at the base of the overlying S-III. It is also present at the base of the S-I. It ranges in volume from about 1 to 3% (Ramm, 1991). Ankerite is present at about 1% in a sample from 2785.5 m (RKB). Calcite and dolomite are totally absent from XRD analysis of the western well 7119/12–1 (Ramm, 1991). Unlike the western well, the eastern wells 7120/9–1 and 7121/7–1 contain calcite cement in amounts ranging from 0.1 to 0.4% for calcite and from 0.2 to 0.7% for dolomite. Siderite is present in the eastern wells but in lesser quantity from 0.1 to 0.4% where available. Ankerites are present as well and range in value from 0.1 to 1.2% where present. Siderite is considered an early diagenetic product which must have precipitated early following or during deposition.

Clay Minerals: Clay minerals observed in the samples include muscovite, illite and kaolinite (Fig. 11a and b). Illite is the most common of these minerals. Where present in thin sections, illite is mostly seen as an authigenic mineral or as clay clasts. This is observed from bulk XRD mineralogy in both the western and eastern wells with amounts ranging from ~1 to ~4% in well 7119/12–1 (Fig. 8a), from 0.8 to 5.3% in well 7120/9–1 (Fig. 8b) and from 0.7 to 6.0% in well 7121/7–1 (Fig. 8c). Bulk XRD analysis of Ramm (1991) for western well 7119/12-1 shows that kaolinites are completely absent but only present in a sample from the base of S-I at 2810.10 m (RKB) with an amount of 9.9%. Kaolinite occurrence is higher although in low amounts in the eastern wells which is in contrast to observation in the western well. In well 7120/9–1, it ranges from 0.4 to 1.1% and from 0.6 to 6.8% in well 7121/7–1. When present, they occur either as pore-filling minerals, feldspar-replacing minerals/kaolinite clasts or in splaying mica. Muscovite (Table 3) is low in the western well and it ranges from 0.3 to 1%

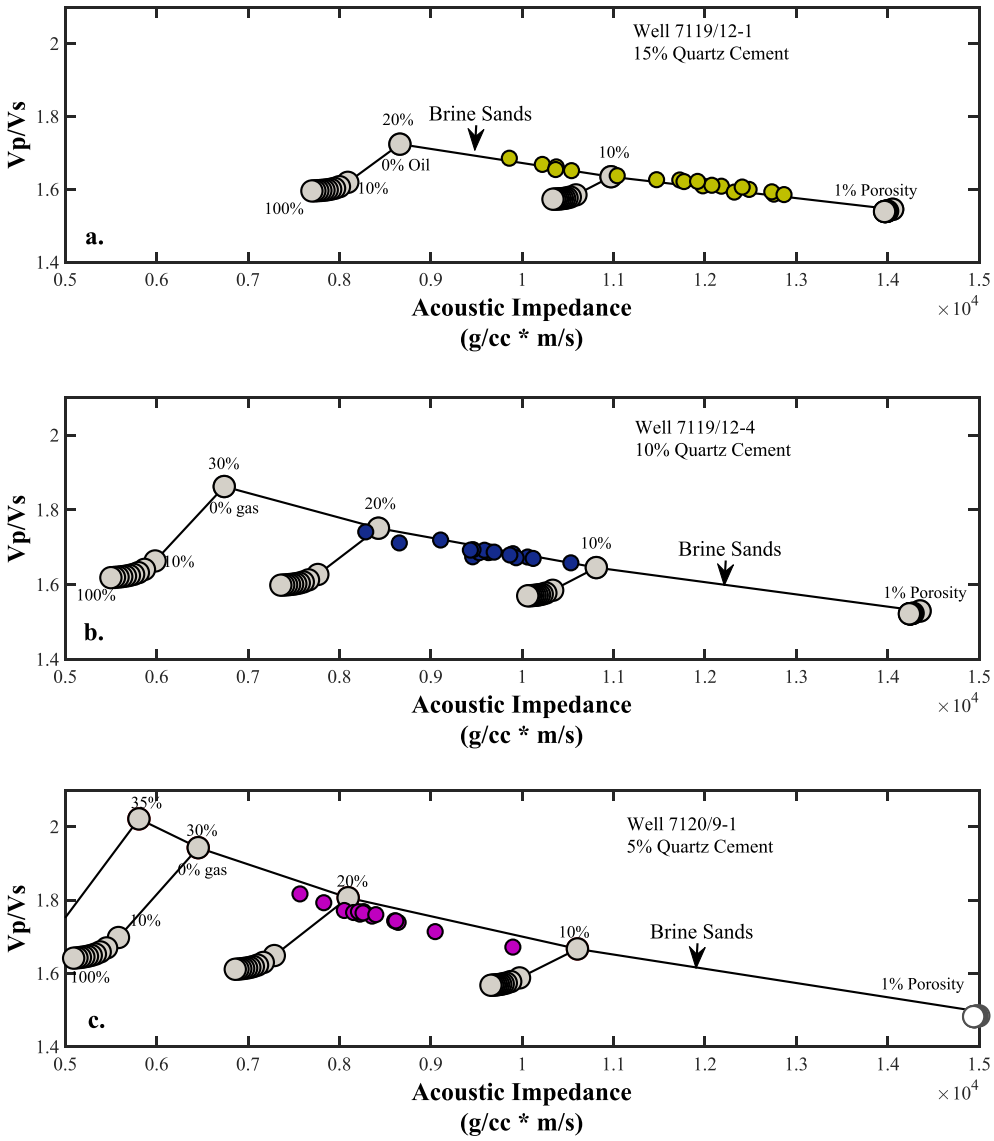

Fig. 7. Rock physics templates of acoustic impedance versus Vp-Vs ratio for wells a) 7119/12–1, b) 7119/12–4 and c) 7120/9–1. Figures a to c show decreasing quartz cement, clay content, acoustic impedance and increasing porosity from the western wells to the eastern wells.

where present, while in eastern well 7120/9–1, no muscovite is observed in thin section (Table 3). In well 7121/7–1, muscovite is present and ranges from 0.3 to 2.6% (Table 4). These muscovites show varying degrees of illitization. XRD analysis does not clearly discriminate between illite and muscovite. This means that muscovite is included in the illite estimate thereby overestimating illite content and underestimating the presence and amount of muscovite.

Accessory Minerals: These are present as a small or negligible fraction of the sandstone grains. Accessory minerals are relatively denser and more resistant to weathering than the dominant silicate minerals of the sandstones. Accessory minerals present in the Stø Formation sandstones include framboidal pyrite, rutile, apatite, zircon, tourmaline, illitized mica, glauconite, chert and fossil fragments. These minerals may be indicative of sediment reworking.

4.2.2. Sandstone texture

The Stø Formation in the three wells generally contains very fine-to medium-grained sandstones and occasionally may contain coarse-grained sandstones. In well 7119/12–1, the sandstones are dominantly well sorted and the grains range from fine to medium size sands. Coarse sandstones are present in the lower Stø unit (S-I) (Tables 3 and 4) and may contain cherts (Olaussen et al., 1984). The eastern wells are finer grained and better sorted at each Stø unit than their corresponding coarser equivalent in the western well 7119/12–1 (Fig. 12). Sorting and grain size show an inverse relation where sorting becomes poorer as grain size increases and vice versa. The relatively poorer sorted sandstones (i.e. moderately sorted) are seen to be common in the medium and coarser lower S-I unit in the three wells. While sandstones from well 7119/12–1 are more rounded to subrounded, those of the eastern wells 7120/9–1 and 7121/7–1 are more subangular to angular. Concave-convex and sutured contacts between quartz grains are common in sandstones of well 7119/12–1 with almost no visible to a fair porosity being present in thin section (Table 3).

4.2.3. Sandstone intergranular volume (IGV) versus quartz cement

IGV ranges from about 7.2% to about 37% in the western well 7119/12–1 with an average of about 25% (Table 3, Fig. 13a). In the eastern well 7120/9–1, IGV ranges from about 18% to about 41% with an average of 29%. In well 7121/7–1, IGV ranges from almost 12%–45% with an average of nearly 30%. The eastern wells have similar IGV ranges and averages (Tables 3 and 4, Fig. 13b). IGV above 40% may be attributed to errors in point-counting and overestimation

Table 3
Summary of result from thin section analysis of wells 7119/12–1 and 7120/9-1.

Well/StØ Unit	Depth		Framework Grains					Clay Fraction				Authigenic Clements			Porosity					
	Deptli	Depth																Grain		Sand
7119/12-1	(mRKB)	(mBSF)	Quartz	Fsp	RF	Muscovite	Opaques	ClayMatrix	IC	PFK	Illite	Qtz	Carb	Pyr	Primary	Secondary	IGV	Size	Sort	Type
S-III	2667.7	2442.7	72.4	0.0	0.0	1.0	0.0	0.3	3.6	0.0	0.0	18.4	0.0	0.0	4.3	0.0	22.7	F	VW	QA
	2671.0	2446.0	62.9	0.6	0.0	0.0	0.0	1.0	5.3	0.0	0.0	27.6	0.0	0.0	2.6	0.0	30.2	M	W	QA
	2676.0	2451.0	68.9	0.0	0.3	0.3	0.0	0.0	5.3 11	0.0	0.0	23.6	0.0	0.0	1.6	0.0	25.2	M	w	QA
	2682.5	2457.5	59.7	0.0	0.0	0.6	0.0	0.3	11.2	0.0	0.3	24.6	0.0	0.0	3.3	0.0	28.2	F	w	QA
	2700.3	2475.3	72.1	0.0	0.6	0.0	0.0	2.0	6.3	0.0	0.0	15.0	0.0	0.0	4.0	0.0	19.0	F	MW	QA
	2702.0	2477.0	63.5	0.6	0.0	0.0	0.0	0.0	4.9	0.0	0.3	11.3	0.0	0.0	19.4	0.0	31.0	F	W	QA
	2705.0	2480.0	65.8	0.0	0.0	0.0	0.0	12.7	8.3	0.0	0.0	3.6	0.0	0.0	9.6	0.0	13.2	F	W	QW
S-II	2720.0	2495.0	72.4	0.0	3.0	0.0	0.0	0.0	1.3	0.0	0.0	2.6	0.0	0.0	20.6	0.0	23.2	M	MW	QA
	2725.0	2500.0	67.3	0.0	0.0	0.0	0.0	24.9	0.6	0.0	0.0	1.3	0.0	2.3	3.6	0.0	7.20	F	W	QW
	2740.0	2515.0	66.4	0.0	0.3	0.0	0.0	8.6	3.0	0.0	0.0	13.3	0.0	0.0	8.3	0.0	21.6	F	W	QA
S-I	2745.0	2520.0	47.6	0.0	0.0	0.0	2.0	26.6	2.6	0.0	0.0	20.3	0.0	0.9	0.0	0.0	21.2	F	MW	QW
	2750.0	2525.0	67.1	0.0	4.0	0.0	0.6	0.3	6.6	0.0	0.0	15.0	0.0	0.0	6.3	0.0	21.3	C	M	QA
	2755.0	2530.0	66.7	0.0	1.0	0.0	0.6	2.0	1.7	0.0	0.0	24.3	0.0	0.6	3.0	0.0	27.9	M	W	QA
	2756.5	2531.5	57.3	1.6	3.3	0.3	2.6	1.3	0.3	0.0	0.0	26.6	0.0	1.3	5.3	0.0	33.2	C	M	QA
	2765.0	2540.0	61.4	2.3	0.0	0.0	0.0	5.7	0.7	0.0	0.0	22.6	0.0	0.0	7.3	0.0	29.9	M	MW	QA
	2768.5	2543.5	71.4	2.0	0.0	0.0	0.0	0.0	0.3	0.0	0.0	8.6	0.0	0.0	17.6	0.0	26.2	M	VW	QA
	2775.0	2550.0	59.1	2.7	0.0	0.0	0.0	0.6	1.0	0.0	0.0	21.3	0.0	0.0	15.3	0.0	36.6	M	MW	QA
	2780.0	2555.0	62.8	3.3	0.0	0.0	0.0	1.6	0.6	0.0	0.0	18.1	0.0	0.0	13.6	0.0	31.7	M	MW	QA
	2785.5	2560.5	54.4	2.3	0.0	0.0	0.0	24.3	0.3	0.0	0.0	18.0	0.0	0.3	0.3	0.0	18.6	VF	W	QW
	2788.9	2563.9	63.4	2.0	0.0	0.0	0.0	5.3	6.6	0.0	0.0	19.6	0.0	0.0	3.0	0.0	22.6	VF	W	QW
7120/9-1																				
S-III	1844.9	1501.9	49.1	0.0	0.0	0.0	0.0	1.6	6.6	0.3	0.0	16.7	0.0	0.0	24.1	1.6	41.1	F	MW	QA
	1852.7	1509.7	64.1	0.3	0.3	0.0	0.0	1.0	3.3	0.0	0.0	13.3	0.0	0.0	16.3	1.3	29.6	F	W	QA
S-II	1861.1	1518.1	56.1	0.0	0.0	0.0	2.3	7.6	9.6	0.0	0.0	12.7	0.0	0.0	11.6	0.0	24.3	VF	W	QW
S-I	1870.9	1527.9	56.8	0.0	0.0	0.0	0.0	1.0	6.3	0.0	0.0	18.0	0.0	0.0	18.0	0.0	36.0	VF	W	QA
	1885.4	1542.4	54.4	0.0	0.0	0.0	2.6	15.3	1.6	0.0	0.0	7.0	0.0	0.0	19.0	0.0	26.0	VF	W	QW
	1891.0	1548.0	71.2	0.0	0.6	0.0	0.6	8.3	1.6	0.3	0.0	5.0	0.3	0.0	12.0	0.0	17.6	M	MW	QA

Abbreviations used include Fsp- Feldspar; RF- Rock Fragments; IC- Illite Clast; PFK- Pore filling Kaolinite; Qtz- Quartz; Carb- Carbonate; Pyr-Pyrite; IGV- Intergranular rock volume; Sort-Sorting. Grain size: F-Fine; VF-Very Fine; M-Medium; C-Coarse. Sorting: VW-Very Well; MW-Moderately Well; W- Well; M-Moderately. Sand type: QA-Quartz Arenite; QW-Quartz Wacke; and FW-Feldspathic Wacke.

Table 4
Summary of result from thin section analysis of well 7121/7-1.

Well	Depth		Framework Grains				Clay Fraction		Authigenic Cements			Porosity					
StØ Unit	Depth(m RKB)	Depth(mBSF)	Quartz	Fsp	RF	Muscovite	Opaques	Clay Matrix	IC	PFK	Illite	Qtz	Carb	Pvr	Primary	Secondary	IGV	Grain Size	Sort	Sand Type
7119/12-1																				
s-m	1851.5	1500.5	54.3	0.0	0.0	1.3	0.0	13.0	7.6	1.6	0.0	10.6	0.0	0.0	9.6	2.0	21.8	F	W	QW
	1856.1	1505.1	33.2	0.0	0.0	2.2	0.0	47.3	5.0	0.6	0.0	10.6	0.0	0.0	0.3	0.8	11.5	VF	W	QW
s-n	1864.0	1513.0	47.0	1.3	0.0	2.6	0.0	2.3	1.0	1.3	0.0	19.0	0.0	0.0	24.3	1.2	44.6	VF	W	QA
S-I	1877.3	1526.3	48.9	0.0	0.0	0.6	0.0	2.6	9.3	0.0	0.0	14.3	0.0	0.0	23.0	1.3	37.3	F	VW	QW
	1880.4	1529.4	43.0	0.0	0.0	1.0	0.0	1.0	14.6	0.3	0.0	9.3	0.0	0.0	30.3	0.5	39.9	VF	VW	QW
	1888.7	1537.7	45.6	0.0	0.0	0.0	0.0	0.6	14.3	0.0	0.0	17.0	0.0	0.0	18.3	4.2	35.3	VF	w	QW
	1900.8	1549.8	61.3	0.0	1.0	0.6	0.0	6.3	0.0	0.0	0.0	4.6	0.0	0.0	19.6	6.6	24.2	C	M	QA
	1902.5	1551.5	62.3	0.0	0.0	0.3	0.0	4.0	0.3	0.0	0.0	3.3	0.0	0.0	29.3	0.5	32.6	M	MW	QA
	1906.6	1555.6	34.6	4.6	0.0	1.3	1.0	6.0	31.0	0.3	0.0	6.6	0.0	0.0	14.0	0.6	20.9	VF	W	FW

Abbreviations med include Fsp- Feldspar: RF- Rock Fragments: IC- Illite Clast: PFK- Pore filling Kaolimte; Qtz- Qiaitz: Carb- Carbonate: Pyr-Pyrite: IGV- Intergranular rock volume; Sort-Sorting. Grain size: F-Fiiie: VF-Veiy Fiiie: M-Mediium: C-Coarse. Solling: VW-Veiy Well: MW-Moderately Well: W- Well: M-Moderately. Sand type: QA-Qnaitz Arenite: QW-Quartz Wacke: and FW-Feldspathic Wacke.

of porosity or cements from thin sections.

Plot of IGV versus quartz cement in Fig. 13a depict the well 7119/12-1 having 60% of the data plotting closer to the quartz cement axis than the IGV axes as separated by the single thick, gray diagonal line. Porosity (parallel diagonal lines) from thin section observation is seen to dominate between 0 and 10% in this well with an average of 7.5%. The eastern wells are plotted together here as their IGVs are quite similar with 60% of the data plotting on the lower part of the diagonal line and closer to the IGV axis. The other 40% plots closer to the quartz cement axes above the gray diagonal separator. In the eastern wells, porosity cluster between 10 and 20% with a few points greater than 20% porosity and averages of 16.9% and 18.7% respectively to the well 7120/9–1 and 7121/7–1 (Fig. 13b). Generally, there is low statistical relationship between IGV and quartz cement with R^2 of 0.42 and 0.35 in the western and eastern wells respectively.

Clay matrix (Fig. 13c and d) shows no direct influence on both IGV and quartz cement in both the eastern and western wells but a relationship is observed with porosity only where clay matrix is greater than 15% of the rock volume. Grain size shows no direct relationship with quartz cement, IGV and porosity in the western well (Fig. 13e) while in the eastern wells (Fig. 13f), quartz cementation in finer grains (grain size > 2Ø) is seen to be greater than 5% and less than 5% quartz cement is observed in coarser grains. Sorting does not seem to show any direct relationship with IGV, porosity or quartz cement in all the wells.

4.2.4. Secondary porosity, core permeability and helium porosity

Secondary porosity is rarely present in the western well 7119/12–1 (Table 3). In the eastern well 7120/9–1, secondary porosity mostly from feldspar dissolution is present and ranges between 0% and 1.6% of the rock volume with an average of 0.5% (Table 3). In well 7121/7–1, secondary porosity ranges from 0% to 6.6% with an average of 2% (Table 4). Horizontal permeability from cores in the western well 7119/12–1 ranges up to a second order of magnitude (Fig. 14a) while it is as high as a fourth order of magnitude in the eastern wells (Fig. 14b). No obvious trend with depth is observed but a disorder/scatter which has no direct dependence on quartz cement, bulk clay volume, grain size or sorting (Fig. 14a, c, e, g) while a linear dependence of permeability is seen with helium porosity in this well (Fig. 14i). A similar observation is seen in the eastern wells (Fig. 14b, d, f, h, j). A localized exemption is seen where an arbitrary linear trend occurs between permeability and depth only where clay content is less than 5% of bulk rock volume. Similar trend can be projected to Fig. 14f and h with grain size and sorting. This localized trend in the eastern wells show decreasing permeability with depth for sandstones with similar bulk clay content, grain size and sorting. Helium porosity ranges from 2 to 15% in the western well while it varies from 12 to 25% in the eastern wells. Although, porosity is generally lower in the western well than in the eastern well, but for the same porosity, permeability is higher in the western well than in the eastern wells.

5. Discussion

5.1. Compaction and sources of quartz cement

Mechanical compaction is seen to dominate at depths of about 2000 m in both the eastern and western wells. This is observed at a temperature of about 70 ^{O}C considering Fig. 3e and f. A difference in gradient is seen in the section above the line and those below the line labelled the transition zone (TZ). Velocity change in the mechanical compaction zone is more gradual with depth while a sharper change of velocity with depth is noticed below the transition zone. Mechanical compaction is a function of effective stress, which we can assume equals the difference between overburden stress and pore pressure. Although, from Fig. 4a and b, the Stø Formation is seen to fall within the chemical compaction zone, the initial influence of mechanical compaction on rock physics properties cannot be disregarded.

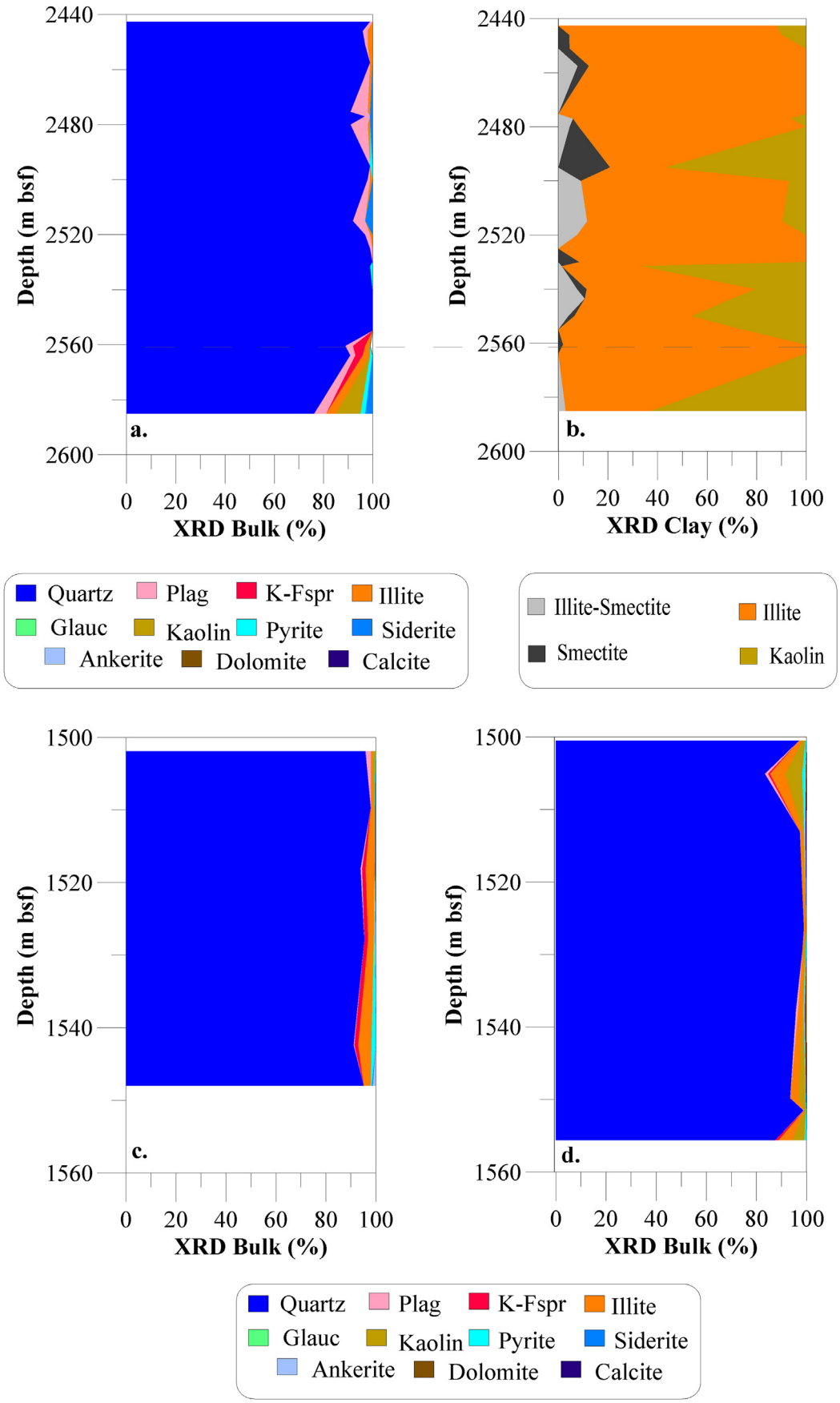

(caption on next page)

Fig. 8. a) XRD bulk mineralogy and b) clay mineralogy for well 7119/12–1. Data used for these plots are semi quantitative representation of data from Ramm (1991); c) XRD bulk mineralogy for wells **7120/9–1 and d**) 7121/7–1. From 2440 m bsf down to about 2560 m bsf, smectite and illite have opposite trends when no K-Feldspar is available. The illite might have formed from the smectite when K-feldspar was originally present to help initiate the smectite-illite reaction as there is a good inverse correlation between smectite and illite. Where K-Feldspar is at its peak (dashed, gray line) and smectite is present at 2560 m bsf, illite is seen to be high as well. Conversely, as the K-feldspar reduces from 2560m bsf to about 2580 m bsf, illite reduces as smectite becomes depleted while plagioclase (albite) increases.

Bjørlykke et al. (1989) explains that porosity preservation at moderate burial depths of less than 3000 m may be an indication of slow rate of porosity loss by mechanical compaction. These may account for the preservation of higher porosities and lower velocities in the eastern rocks which have experienced relatively shallower maximum burial depth (< 3000m) than the western wells (> 3000m). In addition, cementation at such moderate depth may have preserved porosity by supporting the framework grains and hence, inhibiting further compaction and additional porosity loss in the rock. On the other hand, the western wells are more deeply buried and have experienced higher temperatures through time making them more cemented and with corresponding lower porosity (Figs. 4–7).

High velocities in the western wells may also be attributed to the coarser grain size of the sandstones (see Figs. 12 and 13e and f). Coarser grains tend to experience more mechanical compaction and porosity loss (i.e. higher compressibility) and hence, have higher velocities than finer grains (Prasad and Meissner, 1992; Zimmer et al., 2002; Zimmer et al., 2007; Fawad et al., 2011).

Other evidence of the influence of mechanical compaction is seen in deformation styles, fracture development and type and degree of grain to grain contact. Fractures are observed within grains from these sandstones. Investigation under cathodoluminescence as seen in Fig. 10b shows that the grain in Fig. 10a might have been fractured under the influence of overburden stress (mechanical compaction) and these fractures sometimes become healed through quartz cementation infill. Many of these fractures are not visible under plain light and are created as grain to grain contact increases due to exerted overburden stress (Storvoll et al., 2005). They may also form as a result of uplift and associated stress release in the rocks. On the other hand, where less grain to grain contact is observed, grains seem better preserved with

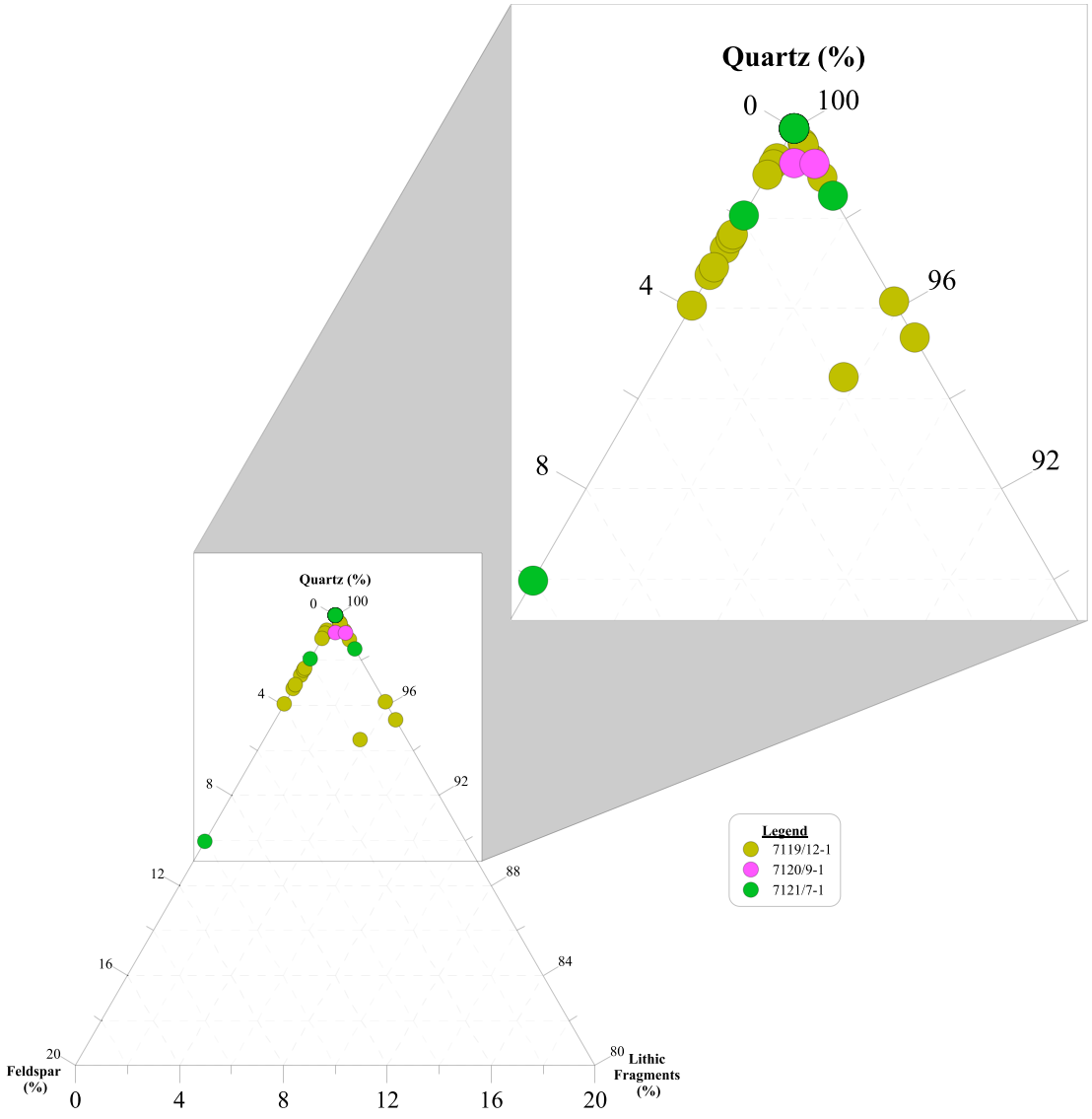

Fig. 9. a) Ternary diagram showing the dominant composition of the Stø Formation in the three wells analysed in thin sections b) zoomed view of upper section of the plot in a). A cluster is seen at the quartz endpoint showing that the sandstones of the Stø Formation are mostly quartz arenites (QA).

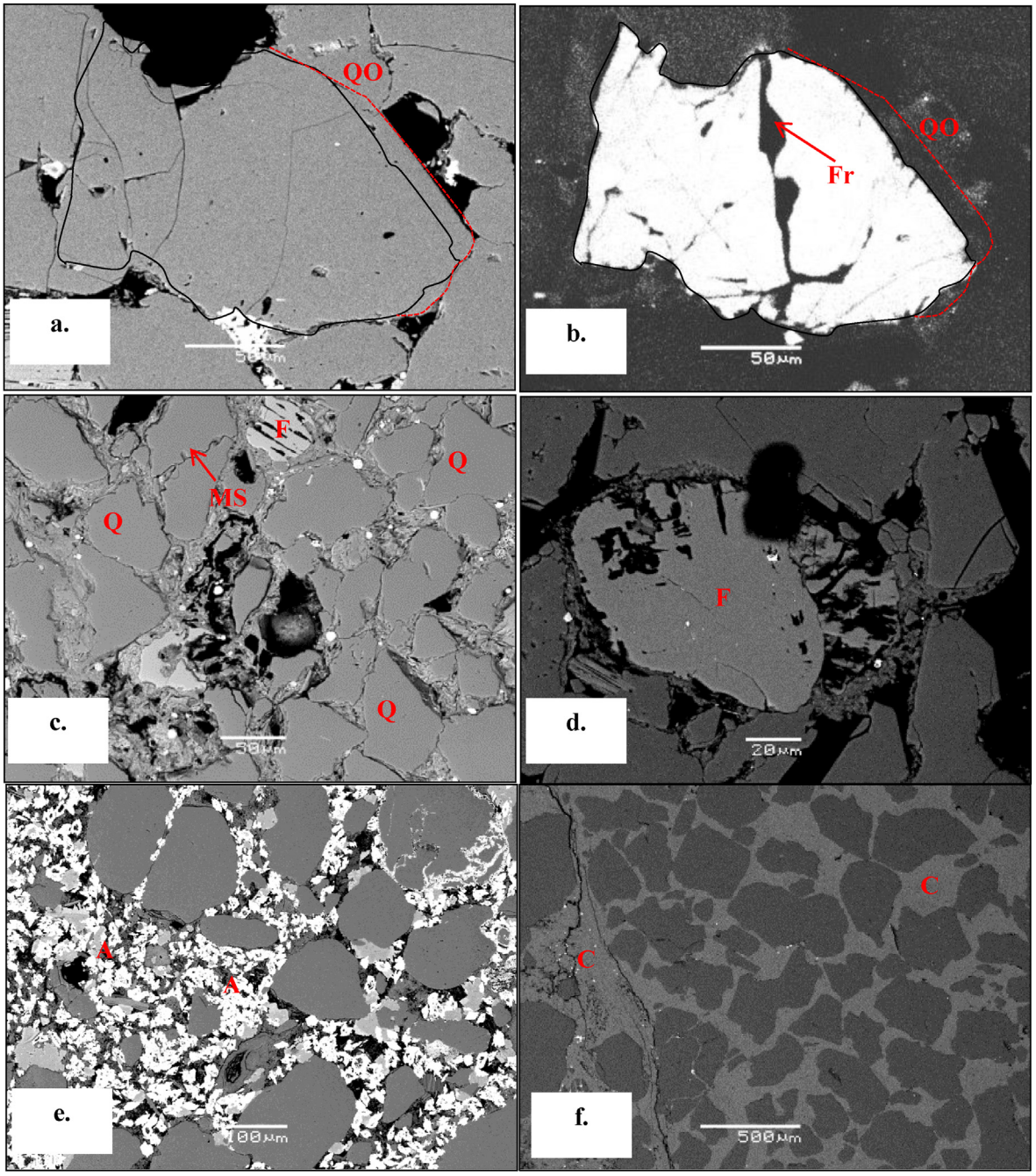

Fig. 10. a) SEM image of fish-shaped detrital quartz grain outlined in dark solid line (1551.8m bsf, well 7120/9–1); while b) highlights the authigenic quartz overgrowth (QO) in red dashed outline. Fr is quartz-healed fracture (in b) which is visible under CL but not obvious in a); c) shows detrital quartz (Q) and feldspar (F) grain along with microstylolites (MS) between quartz grains; d) partially dissolved feldspar grain. Both c) and d) are from 1542.3 m bsf in well 7120/9–1; e) thin section from 1500.52 m bsf of well 7121/7-1 depicts the presence of ankerite (A); f) thin section from 1549.25 m bsf of well 7121/7-1 shows the presence of calcite (C). (For interpretation of the references to colour in this figure legend, the reader is referred to the Web version of this article.)

little or no fracturing. An example of this is seen in Fig. 10e and f where ankerites and calcite respectively fill up the pore space in between framework grains so that there is little room for grains to compact together during mechanical compaction. These show little or no grain to grain contact between the framework grains and as such, little or no grain fracturing is present. This implies that the carbonate cement must have formed early during or immediately after deposition. Presence of fractures within grains may be responsible for the lower velocities in the near-zero porosity, clean quartz-rich sandstones of the western wells.

Type of grain to grain contacts (e.g Fig. 11c and d) ranging from straight through suture to concavo-convex contacts and plastic deformation of ductile minerals (such as the mica sheet in Fig. 11e) are extra evidences of the influence of mechanical compaction on the Stø Formation sandstones. Stress dependent grain to grain crushing of rocks to form finer grains or silt sized grains in between relatively coarser grains is visible in well 7119/12–1 (Fig. 11f). This gives an indication of how high the overburden stress on such a sample might have been.

Chemical compaction on the other hand is a function of the time-temperature integral (TTI). Silicate mineral reactions are very slow and sensitive to temperature. As burial progresses, the influence of temperature through time becomes increasingly important for chemical

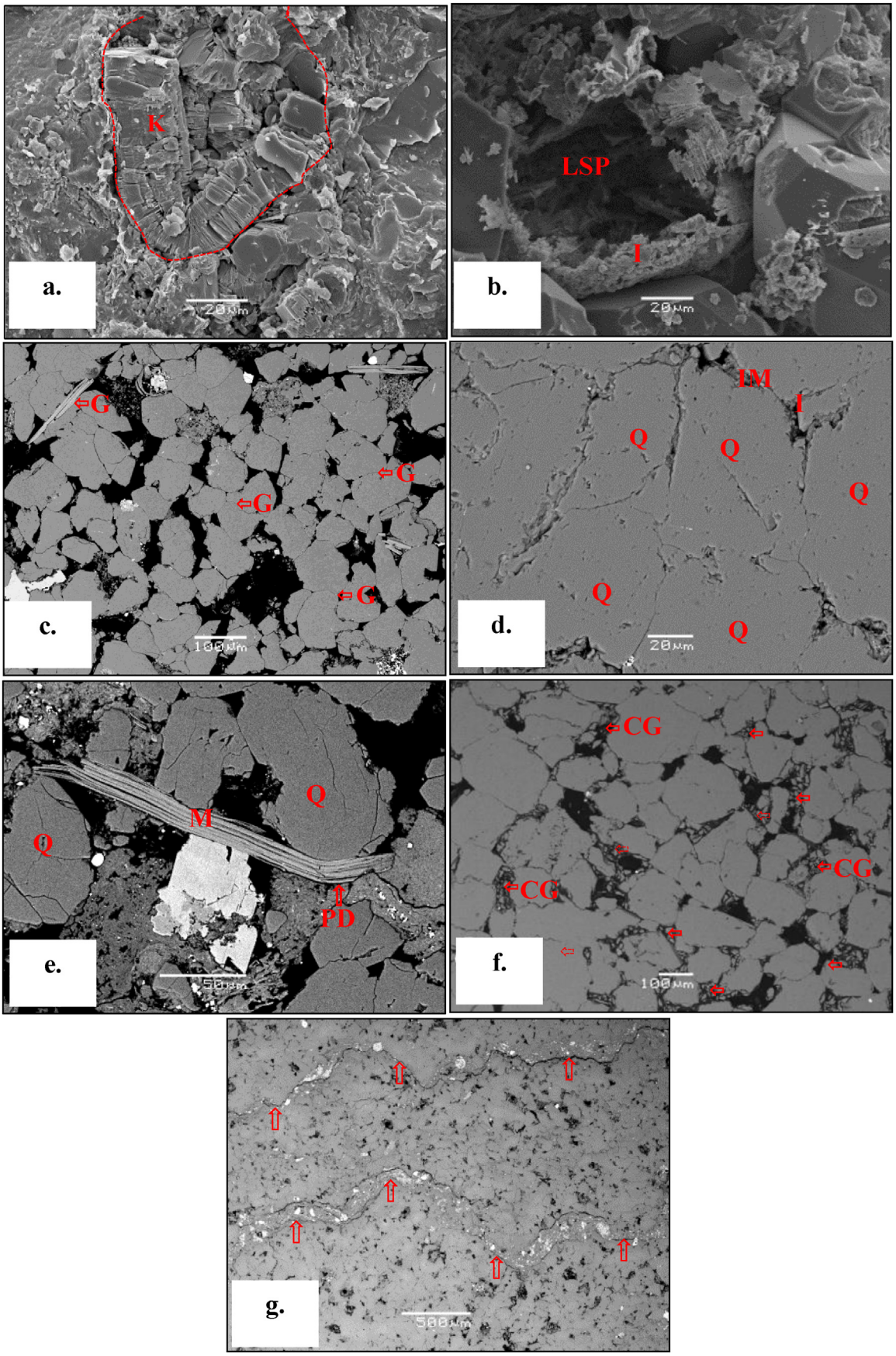

(caption on next page)

Fig. 11. SEM Images of a) kaolinite in a stub of rock sample at 1518.10 m bsf in well 7120/9–1. The red dashed outline shows the grain boundary of possibly feldspar grain; b) shows a large secondary pore (LSP) bounded by illite at 1518.1 m bsf in well 7120/9–1; c) effect of mechanical compaction at grain to grain contacts (G) in a sample from 1526.30 m bsf in well 7121/7–1; d) grain to grain dissolution and interpenetration is observed such that grains cluster and almost look like a single, but fractured grain at 2563.9m bsf in well 7119/12–1; e) plastic deformation (PD) of more ductile muscovite (M) between more brittle minerals such as quartz (Q) from 1526.30 m bsf in well 7121/7–1; f) shows crushed grains (CG) and finer clasts in between coarser grains at 2540m bsf in well 7119/12–1; g) macrostylolites (red arrow) cutting through sandstone at 2520m bsf in well 7119/12–1. (For interpretation of the references to colour in this figure legend, the reader is referred to the Web version of this article.)

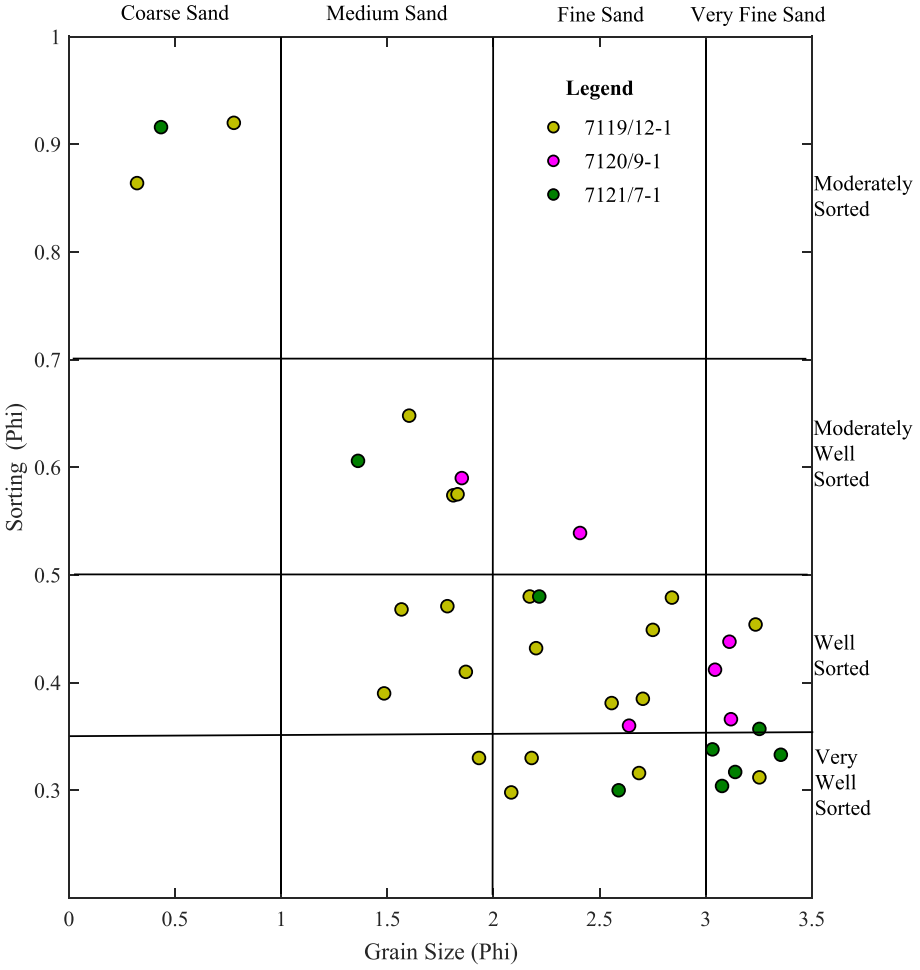

Fig. 12. Textural distribution of the Stø Formation sandstones from wells 7119/12–1, 7120/9–1 and 7121/7–1.

compaction (Bjørlykke, 1998, 2006). The TTI reflects the integrated time and temperature the sediment has experienced above about 70 ^{O}C. Sandstones of the Stø Formation are at present within the chemical compaction regime.

Assuming that depositional IGV is 40% in all the samples, calculations of compactional porosity loss (COPL) and cementational porosity loss (CEPL)(Ehrenberg, 1989) show that nearly 40% of the depositional porosity is lost through compaction in the well 7119/12–1 while 42% of the depositional IGV may have been lost through cementation. Here, cementation only slightly exceeds compaction. This might mean that compactional processes have a close influence on porosity reduction as cementation in the western well. In the eastern wells, COPL and CEPL are respectively 73% and 30% for well 7120/9–1 while they are 75% and 27% respectively in well 7121/7–1. Compaction has a much greater influence on IGV and porosity reduction than cementation in these wells. This implies that while cementation slightly dominated in the western wells, compaction strongly dominated in the eastern wells. This is evidenced in Fig. 13a and b where the western well mostly plot close the quartz cement axis. Whereas, most points in the eastern wells plot close to the IGV axis.

We present a modification from Fig. 7 of Rittenhouse (1971) model in Fig. 13 e and f where the curve is the maximum quartz cement that can be produced internally by CID at grain contacts or microstylolites. These show that most of the sandstones plot as importers of silica from other sources because the silica present as cement exceeds the maximum silica that can be provided by CID at grain contacts. Therefore, CID at grain contacts might have contributed little to compactional loss in the samples and led to little or no corresponding precipitation of cements in the samples. Walderhaug (1994) similarly observed that little dissolution occurs at grain contacts and such dissolution contribute less to silica cement than dissolution at macrostylolites. SEM and cathodoluminescence analysis showed that many of the concave-convex looking contacts are cement-to-cement contacts while only a few contacts showed sutures like microstylolites as shown in Fig. 10c.

Stylolitization is defined here as clay-induced dissolution at macrostylolites and it is identified by constant IGV as quartz cementation varies (Tada and Siever, 1989; Marcussen et al., 2010; Maast and Jahren, 2013). This is possible as pore spaces between adjacent stylolites continually infills with cement dissolved at the stylolite interface, leaving the IGV unaffected. Stylolitization is an important source of

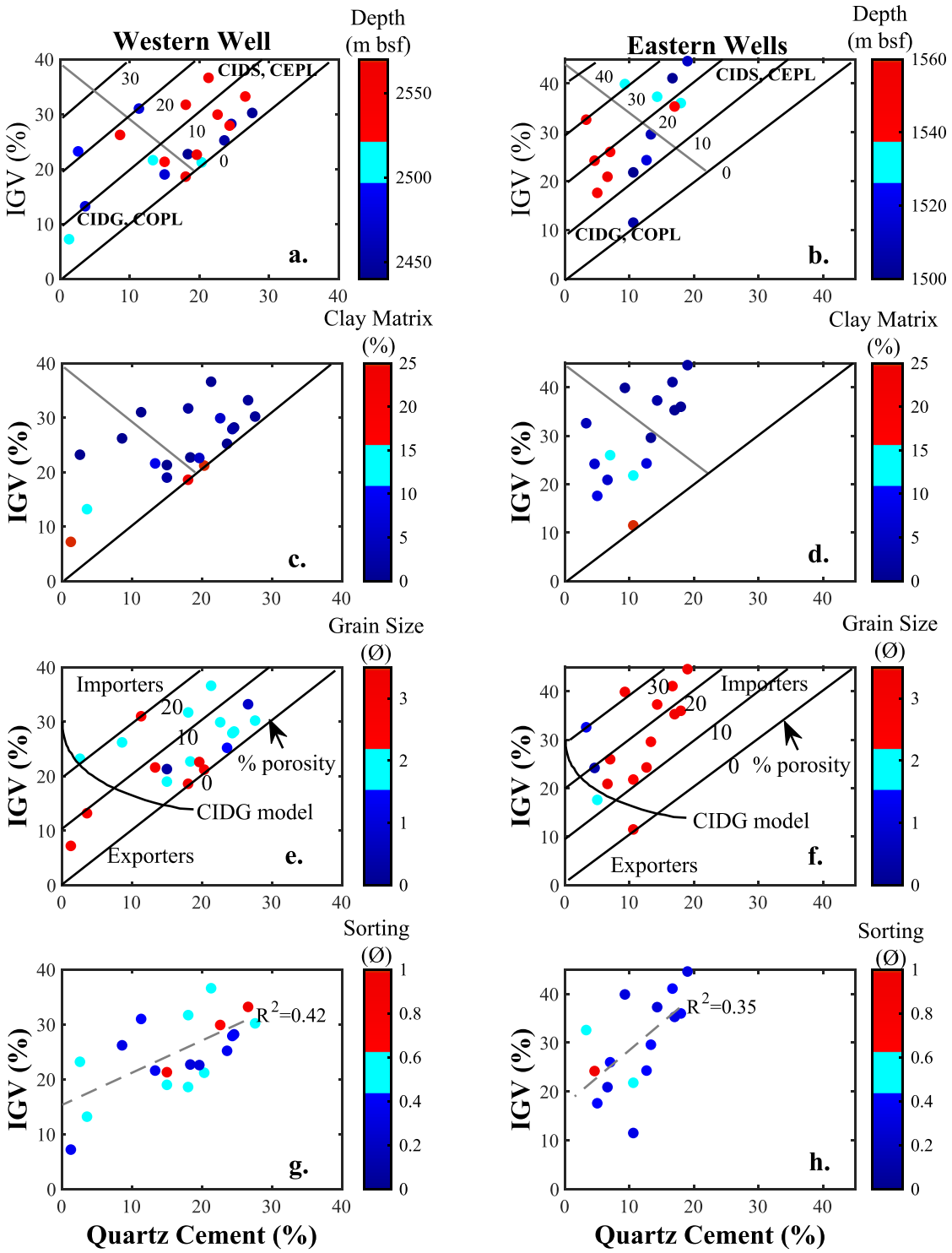

Fig. 13. Quartz cement versus IGV in western well 7119/12–1 (left) and eastern wells 7120/9–1 and 7121/7–1 (right) colour coded by (a,b) depth; (c,d) clay matrix; (e,f) grain size and (g,h) sorting. Figures a to d are modified from Houseknecht (1987) and are useful in evaluating the relative importance of compaction and cementation to porosity development in sandstones. Figures e and f are modified from Fig. 7 of Rittenhouse (1971) and the curve depict maximum cement that can be derived from clay-induced dissolution at grain contacts or microstylolites (CIDG). Importers indicate that the sandstone have more cement (from other sources) than can be derived from dissolutiona at grain contacts while exporters mean that the sandstone has excess cement supplied from dissolution at grain contacts. Diagonal lines represent porosities. CIDS: Clay induced dissolution at macrostylolites; COPL: Compactional porosity loss; CEPL: Cementational Porosity Loss. (For interpretation of the references to colour in this figure legend, the reader is referred to the Web version of this article.)

quartz cement in sandstones of the Stø Formation and these are well developed in the sampled wells and dominate more within finer sandstones layers and occur at closely spaced intervals in cores from the wells. Similar observation was noted by Larese et al. (1984); Olaussen et al. (1984); Bjørlykke et al. (1986) and Walderhaug (1994). The precipitation of quartz cement from stylolites is largely controlled by the distance of the sandstones to the nearest stylolites alongside stylolite spacing (Walderhaug, 1996; Walderhaug and Bjørkum, 2003).

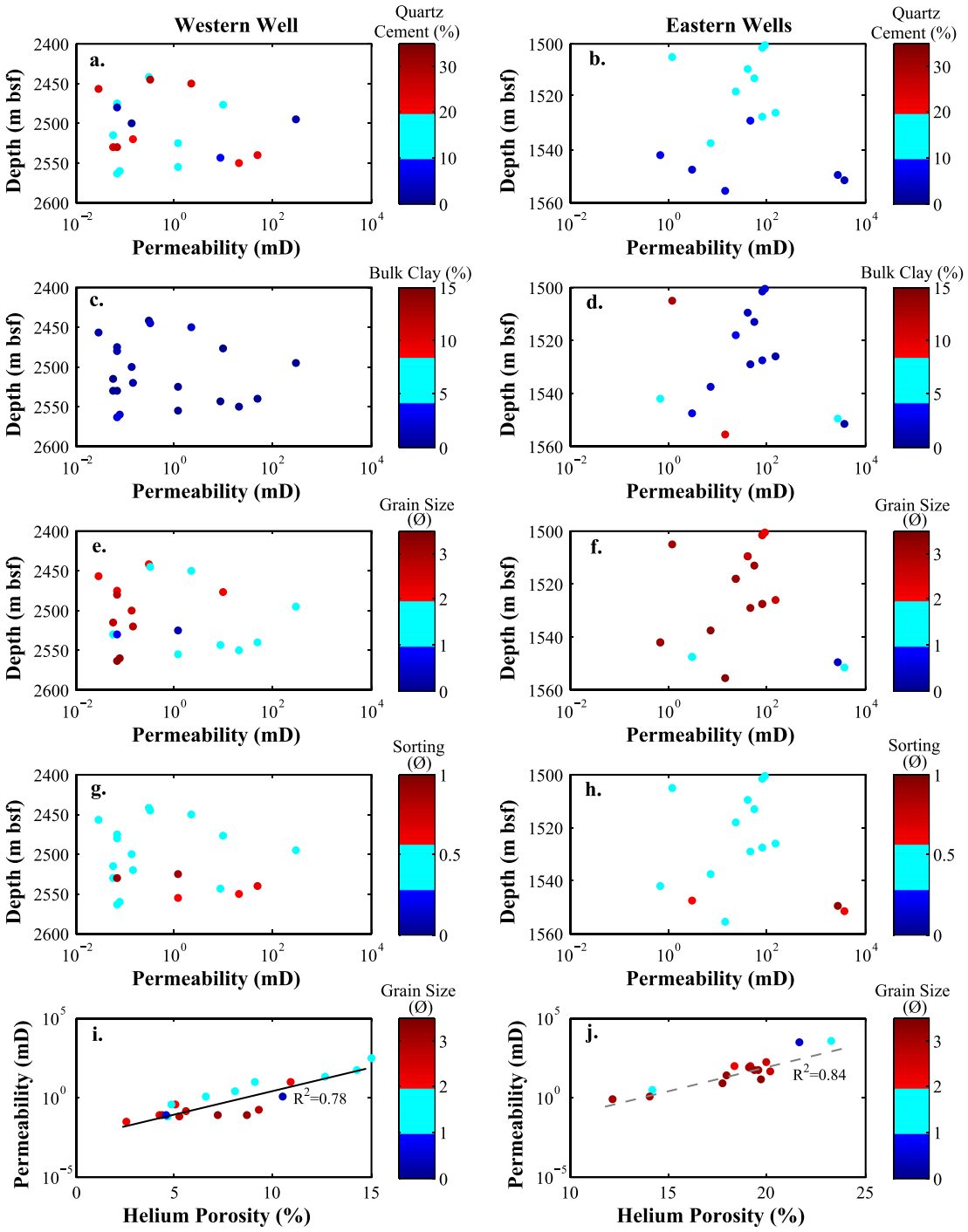

Fig. 14. Plot of horizontal permeability versus present depth in western well 7119/12–1 (left) and eastern wells 7120/9–1 and 7121/7–1 (right) showing variation with a, b) quartz cement; c, d) bulk clay content; e, f) grain size; and g, h) sorting; plots of helium porosity versus horizontal permeability in western well 7119/12–1 (i) and eastern wells 7120/9–1 and 7121/7–1 (j) colour coded by grain size. (For interpretation of the references to colour in this figure legend, the reader is referred to the Web version of this article.)

Observation from core images show that at a distance of less than 2 cm from the nearest stylolite, quartz cementation ranges from approximately 10% to almost 30% while at distance of greater than 2 cm–20 cm, most quartz cement ranges from 1% to less than 10%.

Bjørlykke (1988) suggested the development of microstylolites from clay-induced dissolution (CID) at thin clay laminae at a burial depth of about 2000–3000m while fully developed macrostylolites across sandstones are commonly seen at depths between 3000 and 5000 m. After correcting for exhumation, the maximum burial depths of the top of the Stø Formation as seen in Table 1 is greater than 3000m for the western wells and less than 3000m in the eastern wells.

Other chemical compaction processes and source of quartz cement in sandstones include silicate mineral dissolution and silicate mineral transformation (Stone and Siever, 1996) such as the transformation of smectite to illite at temperatures greater than 70 ^{o}C and the concomitant dissolution and albitization of K-feldspar. In Fig. 8, depletion of smectite seems to correspond with an increase in illite and vice versa along with depletion of feldspar at depths above 2560m bsf while plagioclase is relatively abundant where no K-feldspar is present. Below 2560m bsf where K-feldspar is present but decreasing in content and no

smectite is available, illite content starts to decline while at the same time, plagioclase increases. This shows that the smectite to illite transformation occurs in the presence of K^+. The depletion and dissolution of K-feldspars is also obvious in thin section (Figs. 10d and 11b). The transformation of smectite to illite leads to a precipitation of excess silica as quartz cement (Bjørlykke et al., 1989) as seen in the example in equation (4) below from Worden and Morad (1999).

$$1.242H^+ + 0.393K^+ + 1.58\underset{Smectite}{K_{0.1}Na_{0.1}Ca_{0.2}Mg_{0.4}Fe_{0.4}Al_{1.4}Si_{3.8}O_{10}(OH)_2 . H_2O} = \underset{Illite}{K_{0.55}Mg_{0.2}Fe_{0.15}Al_{2.2}Si_{3.5}O_{10}(OH)_2} + 0.16Na^+ + 0.31Ca^{2+} + 0.43Mg^{2+} + 0.24Fe_2O_3 + \underset{Quartz}{2.47SiO_2} + 2.86H_2O \quad (4)$$

Illitization from smectite releases Na^+, Ca^{2+}, Mg^{2+}, and Fe^{2+} ions that could be important to other diagenetic reactions such as formation of ankerite in the same rock (Worden and Morad, 1999). The presence of carbonate cements in some sandstones hinders the precipitation of quartz overgrowth. Such carbonate-cement bearing sandstones show little or no grain to grain contact between the framework grains. This indicates that the carbonate cement must have formed close to the surface. This is described by Olaussen et al. (1984) as pre-compactional carbonate cementation. The carbonate cement shown in Fig. 10e and f fills up the pore space so there is little room for grains to compact together during mechanical compaction. Illitization from kaolinite in the presence of potassium containing phases like K-feldspar would only take place at temperatures greater than 130 ^{O}C (Bjørlykke et al., 1986). The temperatures in the sandstones of the Stø Formation have not reached 130 ^{O}C in the studied wells. Hence, illitization from kaolinite is ruled out.

Dissolution of detrital feldspars for precipitation of kaolinite is seen to occur only in the eastern wells although this is not as common as what is observed in underlying Nordmela Formation sandstones (not presented in this study) of the three wells. Fig. 11a shows an outline of feldspar grain which is totally altered to kaolinite grains (kaolinization). Large secondary porosity (LSP) may be observed from total dissolution of feldspar as seen in Fig. 11b. In confirmation to our observation, Ehrenberg et al. (1993) also showed that the western well 7119/12–1 contained no kaolinite, an abundance of illite and an absence of dickite compared to a southern well 7119/12–2 (Ehrenberg et al., 1993) which has an abundance of kaolinite, low amount of illite and moderate amount of dickite in the Stø Formation. Ramm (1991) carried out bulk XRD analysis of samples from well 7119/12–1 and observed no kaolinite in the 22 samples analysed while 10–56% kaolin was observed in the underlying Nordmela sandstones. This is in agreement with what is visually observed in thin section microscopic studies although the data from the Nordmela Formation is not shown in this study. The kaolin minerals in the underlying Nordmela Formation sandstones were entirely dickite in the well 7119/12–1 (Ramm, 1991). This means that the underlying Nordmela Formation must have experienced temperatures greater than 90–150 ^{O}C that favours kaolinite-dickite transformation. From exhumation estimates and also from vitrinite analyses, temperatures have reached a maximum of between 100 and 110 ^{O}C. Ramm (1991) suggested from fluid inclusion analysis of a sample from well 7119/12–1 at 2750 m RKB (2525 m bsf) that the quartz cements must have precipitated at least at temperatures between 116 and 125^{O}C. If kaolinites were originally available in the Stø Formation, they should as well still be present at such temperatures. Based on this knowledge, kaolinite is absent in the western well 7119/12–1 which may be related to distal position from the provenance for kaolinite whereas the eastern wells are more proximal to the kaolinite source.

The creation of secondary porosity may or may not necessarily change the total porosity. If what is being dissolved is of greater volume than what is precipitated, then the total porosity may increase. In well 7120/9–1 for example, 2.9% secondary porosity is observed while only 0.6% of pore filling kaolinite has been formed from feldspar alteration (Table 3). The dissolution of feldspar in this well enhances the total porosity. Consequently, the presence of kaolinite in the sandstones may only slightly hinder due to its small particle size or otherwise slightly enhance permeability due to the slightly more porous and permeable booklet nature of the kaolinite. Similarly, in the well 7121/7–1, it seems that 4.1% of pore filling kaolinite was formed from dissolution while an excess of 17.7% residual secondary porosity is created (Table 4). The presence of greater volume of secondary porosity in the eastern wells help to enhance the total porosity and this in turn gives the sandstone a better reservoir quality than those of the western well where no visible secondary porosity coupled with only fair porosity is observed.

Based on the depth suggestions of Bjørlykke (1988) along with evidences earlier discussed, the dominant source of quartz cement in the western well 7119/12–1 is clay induced dissolution at macrostylolites (as seen in Fig. 11g) and less from microstylolites. For the eastern wells, the quartz cement is dominantly sourced from clay induced dissolution at microstylolites (e.g Fig. 10c) and less from macrostylolites. Additional sources of quartz cement in both wells are silicate mineral dissolution and transformation.

5.2. Rock physics interpretation

A comparison between our data and the rock physics models (Figs. 5 and 6) show that the sandstones are cemented which supports what is observed from thin section and stub analyses. The sandstones from the eastern and western wells show distinct Vp-porosity cluster which becomes clearer in Vs-porosity plot. Vs is not influenced by fluid effect and this is the reason for a clearer trend which can subsequently be attributed to lithologic or textural effect. The variation in velocity-porosity trend is diagnosed using constant cement and contact cement models along with the methods of estimation of cementation provided by Dvorkin and Brevik (1999) and Hossain and MacGregor (2014). The velocity-porosity plot in Fig. 6a, b and c show that the western wells are diagenetically more mature with more quartz cements than the eastern wells and Fig. 6c show the western wells being more proximal to the quartz end point and to the Voigt upper bound that depicts the stiffest possible bound.

The contact cement model represents the initial stage of diagenesis while the constant cement model is a line of constant age or depth with decreasing sorting from the critical porosity to the mineral endpoint (Avseth et al., 2010a, 2010b). As diagenesis progresses and cementation becomes more intense, modified upper Hashin Shtrikman bound is applied as it works best in modelling increasing cement in the rock (Avseth et al., 2010a, 2010b). Fig. 6b shows that the western wells are generally more quartz cemented than the eastern wells although contact cement may be least in most part of the western well 7119/12–1. Small quantities of cements at grain contacts have been evidenced to cause a dramatic increase in rock stiffness and velocity of granular rocks (Dvorkin and Nur, 1996; Dvorkin et al., 1994; Vernik and Nur, 1992). This would mean that the greater amount of cement especially quartz cement, which is dominant in these samples, contributes to the higher velocities observed in the western wells than what is seen in sandstones of the eastern wells with less amount of cementation. A combination of higher grain-to-grain point contacts per grain (due to the influence of mechanical compaction) with higher quartz cement coupled with decreasing porosity as clay volume increases is a recipe for much increased velocity. Contact cementation even in limited quantity would easily strengthen the rock framework and reduce the influence of mechanical compaction as overburden stress increases (Bjørlykke, 1988). The reduced effect of mechanical compaction combined with less quartz cement and better sorting might be the reason for better porosity preservation in the eastern wells. As we go from the east

to west, the rocks or pores become stiffer with decreasing sorting, increased compaction and increased cementation.

Reduction of acoustic impedance from the western well to the eastern wells in Fig. 7 is due to reduced cementation from the western wells to the eastern wells according to the modelling. Modelled high quartz cement volume in the sandstones of the western well 7119/12–1 causes a significant stiffening in the rock framework and subsequently reduces the fluid sensitivity (Avseth et al., 2009). This is the reason for the oil saturated sandstones sitting on the brine sand line. On the other end, the eastern well 7120/9-1 modelled with less quartz cement than the western well experiences an improvement in the fluid sensitivity so that gas saturated sandstones are located within the gas zone beneath the brine saturated line. In the intermediate well with moderate quartz cement, the brine saturated sandstones lie on the brine sand line.

A dependence of permeability on porosity is shown in Fig. 14i and j. Pore geometry has an effect on permeability (Hartmann and Beaumont, 1999). This effect is explained by rock physics diagnostics in Fig. 6d where slightly higher permeabilities are observed in the generally low porosity western well than in the high porosity eastern wells. This anomaly is highlighted in the red boxes in Fig. 6. Outside the anomaly, where porosity is less than 10%, rock physics diagnostics indicate low contact cement (1–5%) and poorer sorting in the well 7119/12–1. Deteriorating sorting along each constant cement line can be due to increased pore-filling or non-contact cement that causes an increase in specific surface area which consequently reduces permeability (Dvorkin and Brevik, 1999; Avseth et al., 2000 and references herein) hence, the reason for low permeability in the low porosity sandstones of well 7119/12–1. On the other hand, in the anomalous zone highlighted by the red rectangle, at porosity between 10 and 20%, contact cement is slightly higher in the western well 7119/12–1 than in the eastern wells for same porosity. On the contrary, the eastern wells have a slightly lower contact cement. Non-contact or pore-filling material which reduces sorting and occupies the porespace is slightly higher (see Fig. 5 e, f, h) in the eastern wells and therefore lowers the permeability in these wells.

Fig. 5e–h shows lower shale volume in the western wells (except 7019/1-1) than in the eastern wells. Slightly higher volume of contact cement combined with lower shale volume in the western well within this porosity region causes a dramatic increase in velocity while lower volume of contact cement coupled with higher shale volume leads to lower velocity in the eastern well at similar porosity (see Fig. 6b and d).

Although, no good correlation is observed between bulk clay content, grain size and sorting with permeability (Fig. 14), each factor can still highly affect permeability, but the effect is not clearly seen due to the competing effect of one factor over another in these sandstones.

6. Conclusions

The Jurassic Stø Formation sandstones in the Barents Sea are very fine to medium grained and occasionally coarse grained in lower parts of the formation. These very well to moderately well sorted quartz arenitic sandstones were deposited in a high energy shoreface/foreshore environment. Sandstones in wells from three sub-basins including the Hammerfest Basin, Ringvassøy-Loppa Fault Complex and the Troms-Finnmark Fault Complex have been studied for mechanical and chemical compaction and their influence on reservoir quality of these sandstones. Important observations in this study are summarized below:

- Exhumation decreases westward from the east with well 7121/7–1 in the Hammerfest Basin being the most exhumed (1050 m) and well 7019/1-1 of the Troms-Finnmark Fault Complex being the least exhumed (820 m). After exhumation correction, the top of the Stø Formation sandstones in well 7119/12–1 is the most deeply buried at about 3500 m RKB followed by wells 7019/1-1, 7119/12–4, 7121/7–1 and the least buried being well 7120/9–1 at a maximum burial depth of about 2820 m RKB. The estimated maximum temperature which the Stø Formation experienced is higher in the western wells (~110–~130 ^{O}C) than in the eastern wells (~90–~100^{O}C).
- Difference in burial history and textural variations between sandstones from the different sub-basins have huge effect on compaction and cementation of the Stø sandstones. Sandstones from the western wells are more deeply buried, more stiff, compacted and cemented than the eastern wells. A combination of higher grain-to-grain point contacts per grain (due to the influence of mechanical compaction) with higher quartz cement coupled with decreasing porosity as clay volume increases is a recipe for much increased velocity in the western wells. Contact cementation even in limited quantity easily strengthens the rock framework and reduces the influence of mechanical compaction as overburden stress increases. The reduced effect of compaction combined with less quartz cement and better sorting might be the reason for better porosity preservation in the eastern wells.
- Rock physics models and diagnostics show that the western wells are diagenetically more mature with more quartz cements than the eastern wells. The western wells are more proximal to the quartz end point and to the Voigt upper bound that depicts the stiffest possible bound.
- Compressional wave velocity (Vp) is higher in the more deeply buried western well and ranges between 4000 and 5000 m/s. In the eastern well on the other hand, Vp ranges between 3500 and 4000 m/s. For clean sandstones with near zero-porosity in the western wells, Vp is expected to be close to 6000 m/s but this is not the case. The relatively lower velocities may be attributed to the presence of microfractures within the grains that might have generated during uplift episodes and consequent stress release in the rock.
- Cementation prevails over compaction in the western wells while compaction strongly dominates over cementation in the eastern wells. The most important source of quartz cement in the western well 7119/12–1 is clay induced dissolution at macrostylolites and less from microstylolites while in the eastern wells, the quartz cement are dominantly sourced from clay induced dissolution at microstylolites and less from macrostylolites. Additional sources of quartz cement in both wells are silicate mineral dissolution and transformation.
- Permeability is generally higher in the eastern wells than in the western wells, but at similar porosities, permeability is higher in the western wells than in the eastern wells. Pore geometry defines permeability distribution in these wells with increased pore-filling or non-contact materials causing an increase in specific surface area which in turn reduces permeability and vice versa.
- The individual effect of bulk clay volume, grain size and sorting on permeability is difficult to observe because of the competing effect of all these factors along with compaction and cementation on the Stø Formation sandstones.

7. Recommendations for future work

For a more comprehensive understanding of the Stø sandstones, we recommend detailed study on the three units of the Stø Formation. Pressure regimes and their impact on compaction and cementation should be carried out in addition to more rigorous rock physics analyses for these sandstones. In addition to these, quartz cement modelling using Walderhaug (1996) diagenetic model for burial history and comparison with thin section and rock physics analysis would contribute significantly to these studies.

CRediT authorship contribution statement

Oluwakemi Yetunde Ogebule: Methodology, Software,

Validation, Formal analysis, Investigation, Writing - original draft, Writing - review & editing, Visualization. **Jens Jahren:** Supervision, Funding acquisition, Conceptualization, Methodology, Resources, Writing - original draft, Writing - review & editing. **Nazmul Haque Mondol:** Supervision, Funding acquisition, Conceptualization, Methodology, Resources, Writing - original draft, Writing - review & editing.

Declaration of competing interest

The authors declare that they have no known competing financial interests or personal relationships that could have appeared to influence the work reported in this paper.

Acknowledgements

Our appreciation goes to The Research Council of Norway, Oslo, Norway for funding the research on BarRock (Barents Sea Rock Properties) project through the PETROMAKS2 Programme. Many thanks to Mogens Ramm for permitting us to use data from his PhD Thesis. Our deepest gratitude goes to the technical staff at the Department of Geosciences, University of Oslo for their support with the use of SEM and XRD setups. Finally, we are grateful to the Norwegian Petroleum Directorate for making available the data used in this study through Diskos National Data Respository (NDR). We appreciate the reviewers for their comments and suggestions which better improved the manuscripts.

Appendix

Workflow Diagram for Stø Formation Sandstones.

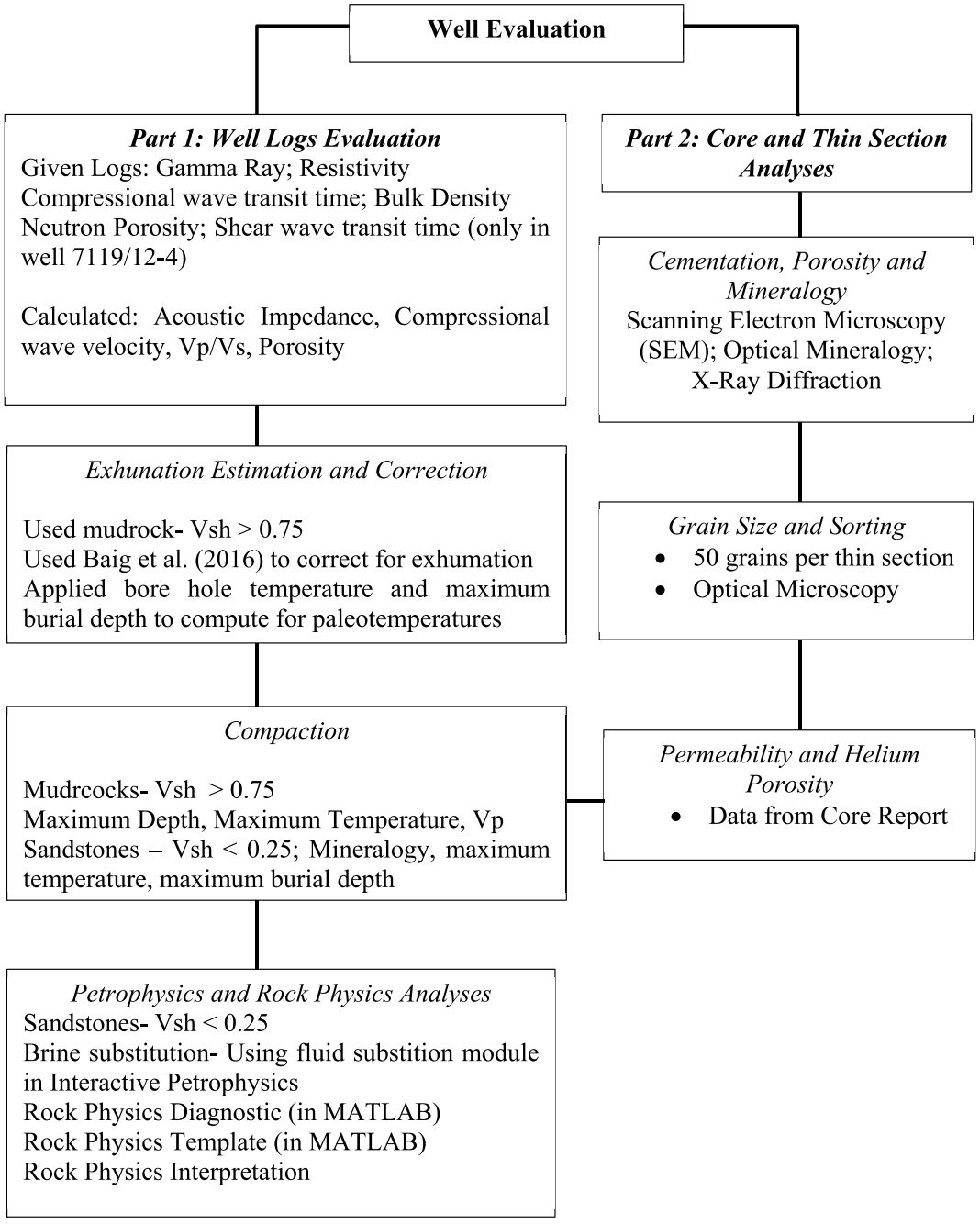

Appendix A. Supplementary data

Supplementary data to this article can be found online at https://doi.org/10.1016/j.marpetgeo.2020.104448.

References

Aase, N.E., Bjørkum, P.A., Nadeau, P.H., 1996. The effect of grain-coating microquartz on preservation of reservoir porosity. AAPG Bull. 80, 1654–1673.

Ali, S.A., Clark, W.J., Dribus, J.R., 2010. Diagenesis and reservoir quality. Oilfield Review Summer 22 (2), 14–27.

Asquith, G.B., Krygowski, D., Henderson, S., Hurley, N., 2004. American Association of Petroleum Geologists. second ed. American Association of Petroleum Geologists, Tulsa, Okla Basic well log analysis.

Avseth, P., Dvorkin, J., Mavko, G., Rykkje, J., 2000. Rock physics diagnostics of North Sea sands: link between microstructure and seismic properties. Geophys. Res. Lett. 27, 2761–2764.

Avseth, P., Jørstad, A., Wijngaarden, A.-J.v., Mavko, G., 2009. Rock physics estimation of cement volume, sorting, and net-to-gross in North Sea sandstones. Lead. Edge 28, 98–108.

Avseth, P., Mukerji, T., Mavko, G., 2010. Quantitative Seismic Interpretation: Applying Rock Physics Tools to Reduce Interpetation Risk. Cambridge university press, pp. 359pp.

Avseth, P., Mukerji, T., Mavko, G., Dvorkin, D., 2010b. Rock-physics diagnostics of depositional texture, diagenetic alterations, and reservoir heterogeneity in high-porosity siliciclastic sediments and rocks- A review of selected models and suggested work flows. Geophysics 75, 75A31–75A47.

Baig, I., Faleide, J.I., Jahren, J., Mondol, N.H., 2016. Cenozoic exhumation on the southwestern Barents Shelf: estimates and uncertainties constrained from compaction and thermal maturity analyses. Mar. Petrol. Geol. 73, 105–130.

Batzle, M., Wang, Z., 1992. Seismic properties of pore fluids. Geophysics 57, 1396–1408.

Berglund, L.T., Augustson, J., Færseth, R., Gjelberg, J., Ramberg-Moe, H., 1986. The Evolution of the Hammerfest Basin. Norwegian Petroleum Society, pp. 319–338.

Berryman, J.G., 1995. Mixture theories for rock properties. In: Ahrens, T.J. (Ed.), Rock Physics and Phase Relations: A Handbook of Physical Constants. American Geophysical Union, Washington, pp. 205–228.

Bjørkum, P.A., 1996. How important is pressure in causing dissolution of quartz in sandstones? J. Sediment. Res. 66, 147–154.

Bjørkum, P.A., Oelkers, E.H., Nadeau, P.H., Walderhaug, O., Murphy, W.M., 1998. Porosity prediction in quartzose sandstones as a function of time, temperature, depth, stylolite frequency, and hydrocarbon saturation. AAPG Bull. 82, 637–648.

Bjørlykke, K., 1988. Chapter 2 sandstone diagenesis in relation to preservation, destruction and creation of porosity. In: Chilingarian, G.V., Wolf, K.H. (Eds.), Dev. Sedimentol. Elsevier, pp. 555–588.

Bjørlykke, K., 1998. Clay mineral diagenesis in sedimentary basins - a key to the prediction of rock properties. Examples from the North Sea Basin. Clay Miner. 33, 15–34.

Bjørlykke, K., 2006. Effects of compaction processes on stresses, faults, and fluid flow in sedimentary basins: examples from the Norwegian margin. In: Buiter, S.J.H., Schreurs, G. (Eds.), Analogue and Numerical Modelling of Crustal-Scale Processes, pp. 359–379.

Bjørlykke, K., Aagaard, P., Dypvik, H., Hastings, D.S., Harper, A.S., 1986. Diagenesis and reservoir properties of Jurassic sandstones from the Haltenbanken area, offshore mid-Norway. In: Spencer, A.M. (Ed.), Habitat of Hydrocarbons on the Norwegian Continental Shelf. Graham & Trotman, London, pp. 275–286.

Bjørlykke, K., Chuhan, F., Kjeldstad, A., Gundersen, E., Lauvrak, O., Høeg, K., 2004. Modelling of sediment compaction during burial in sedimentary basins. In: Ove, S. (Ed.), Elsevier Geo-Engineering Book Series. Elsevier, pp. 699–708.

Bjørlykke, K., Egeberg, P.K., 1993. Quartz cementation in sedimentary basins. AAPG Bull. 77, 1538.

Bjørlykke, K., Jahren, J., 2010. Sandstones and Sandstone Reservoirs, Petroleum Geoscience: from Sedimentary Environments to Rock Physics. Springer Berlin Heidelberg, Berlin, Heidelberg, pp. 113–140.

Bjørlykke, K., Nedkvitne, T., Ramm, M., Saigal, G.C., 1992. Diagenetic processes in the brent group (middle jurassic) reservoirs of the north sea: an overview. Geological Society, London, Special Publications 61, 263–287.

Bjørlykke, K., Ramm, M., Saigal, G.C., 1989. Sandstone diagenesis and porosity modification during basin evolution. Geol. Rundsch. 78, 243–268.

Blott, S.J., Pye, K., 2001. GRADISTAT: a grain size distribution and statistics package for the analysis of unconsolidated sediments. Earth Surf. Process. Landforms 26, 1237–1248.

Chuhan, F.A., Kjeldstad, A., Bjorlykke, K., Hoeg, K., 2003. Experimental compression of loose sands: relevance to porosity reduction during burial in sedimentary basins. Can. Geotech. J. 40, 995–1011.

Chuhan, F.A., Kjeldstad, A., Bjørlykke, K., Høeg, K., 2002. Porosity loss in sand by grain crushing—experimental evidence and relevance to reservoir quality. Mar. Petrol. Geol. 19, 39–53.

Densley, M.R., Hillis, R.R., Redfearn, J.E.P., 2000. Quantification of uplift in the Carnarvon Basin based on interval velocities. Aust. J. Earth Sci. 47, 111–122.

Dimakis, P., Braathen, B.I., Faleide, J.I., Elverhoi, A., Gudlaugsson, S.T., 1998. Cenozoic erosion and the preglacial uplift of the Svalbard-Barents Sea region. Tectonophysics 300, 311–327.

Dræge, A., 2011. A diagenetic rock physics approach for siliciclastics. Lead. Edge 30, 1368–1375.

Dvorkin, J., Brevik, I., 1999. Diagnosing high-porosity sandstones; strength and permeability from porosity and velocity. Geophysics 64, 795–799.

Dvorkin, J., Nur, A., 1996. Elasticity of high-porosity sandstones: theory for two North Sea data sets. Geophysics 61, 1363–1370.

Dvorkin, J., Nur, A., Yin, H.Z., 1994. Effective properties of cemented granular-materials. Mech. Mater. 18, 351–366.

Ehrenberg, S.N., 1989. Assessing the relative importance of compaction processes and cementation to reduction of porosity in sandstones; discussion; Compaction and porosity evolution of Pliocene sandstones, Ventura Basin, California; discussion. AAPG Bull. 73, 1274.

Ehrenberg, S.N., Aagaard, P., Wilson, M.J., Fraser, A.R., Duthie, D.M.L., 1993. Depth-dependent transformation of kaolinite to dickite in sandstones of the Norwegian Continental-Shelf. Clay Miner. 28, 325–352.

Faleide, J.I., Vågnes, E., Gudlaugsson, S.T., 1993. Late Mesozoic-Cenozoic evolution of the south-western Barents Sea in a regional rift shear tectonic setting. Mar. Petrol. Geol. 10, 186–214.

Fawad, M., Mondol, N.H., Jahren, J., Bjorlykke, K., 2011. Mechanical compaction and ultrasonic velocity of sands with different texture and mineralogical composition. Geophys. Prospect. 59, 697–720.

Gabrielsen, R.H., Færseth, R., Hamar, G., Rønnevik, H., 1984. Nomenclature of the main structural features on the Norwegian Continental Shelf north of the 62nd parallel. In: Spencer, A.M. (Ed.), Petroleum Geology of the North European Margin: Proceedings of the North European Margin Symposium (NEMS '83), Organized by the Norwegian Petroleum Society and Held at the Norwegian Institute of Technology (NTH) in Trondheim 9–11 May, 1983. Springer Netherlands, Dordrecht, pp. 41–60.

Gabrielsen, R.H., Færseth, R.B., Jensen, L.N., Kalheim, J.E., Riis, F., 1990. Structural elements of the Norwegian continental shelf. Part 1: the Barents Sea region. 6. Norwegian Petroleum Directorate, pp. 1–33.

Gassmann, F., 1951. Uber die elastizitat poroser medien. Vier. Natur Gesellschaft 96, 1–23.

Giles, M.R., 1997. Diagenesis: A Quantitative Perspective- Implications for Basin Modelling and Rock Property Prediction, 1 ed. Springer Netherlands.

Glørstad-Clark, E., Faleide, J.I., Lundschien, B.A., Nystuen, J.P., 2010. Triassic seismic sequence stratigraphy and paleogeography of the western Barents Sea area. Mar. Petrol. Geol. 27, 1448–1475.

Greenberg, M.L., Castagna, J.P., 1992. Shear-wave estimation in porous rocks: theoretical formulation, preliminary verification and applications. Geophys. Prospect. 40 (2), 195–209. https://doi.org/10.1111/j.1365-2478.1992.tb00371.x.

Han, D., Nur, H., Morgan, D., 1986. Effects of porosity and clay content on wave velocities in sandstones. Geophysics 51, 2093–2107.

Hansen, S., 1996. Quantification of net uplift and erosion on the Norwegian shelf south of 66 degrees N from sonic transit times of shale. Nor. Geol. Tidsskr. 76, 245–252.

Hartmann, D.J., Beaumont, E.A., 1999. Predicting reservoir system quality and performance. In: Beaumont, E.A., Foster, N.H. (Eds.), Treatise of Petroleum Geology/Handbook of Petroleum Geology: Exploring for Oil and Gas Traps. The American Association of Petroleum Geologists 9-1 - 9-154.

Hashin, Z., Shtrikman, S., 1963. A variational approach to the theory of the elastic behaviour of multiphase materials. J. Mech. Phys. Solid. 11, 127–140.

Heald, M.T., 1955. Stylolites in sandstones. J. Geol. 63, 101–114.

Henriksen, E., Bjørnseth, H.M., Hals, T.K., Heide, T., Kiryukhina, T., Kløvjan, O.S., Larssen, G.B., Ryseth, A.E., Rønning, K., Sollid, K., Stoupakova, A., 2011. Chapter 17 Uplift and erosion of the greater Barents Sea: impact on prospectivity and petroleum systems. Geological Society 35, 271–281 London, Memoirs.

Hossain, Z., MacGregor, L., 2014. Advanced rock-physics diagnostic analysis: a new method for cement quantification. Lead. Edge 33, 310–316.

Houseknecht, D.W., 1984. Influence of grain size and temperature on intergranular pressure solution, quartz cementation, and porosity in a quartzose sandstone. J. Sediment. Petrol. 54, 348–361.

Houseknecht, D.W., 1987. Assessing the relative importance of compaction processes and cementation to reduction of porosity in sandstones. AAPG Bull. 71, 633–642.

Houseknecht, D.W., 1988. Intergranular pressure solution in four quartzose sandstones. J. Sediment. Petrol. 58, 228–246.

James, W.C., Wilmar, G.C., Davidson, B.G., 1986. Role of quartz type and grain size in silica diagenesis, Nugget Sandstone, south-central Wyoming. J. Sediment. Petrol. 56, 657–662.

Larese, R.E., Haskell, N.L., Prezbindowski, D.R., Beju, D., 1984. Porosity development in selected Jurassic sandstones from the Norwegian and North Seas, Norway — an overview. In: Spencer, A.M. (Ed.), Petroleum Geology of the North European Margin: Proceedings of the North European Margin Symposium (NEMS '83), Organized by the Norwegian Petroleum Society and Held at the Norwegian Institute of Technology (NTH) in Trondheim 9–11 May, 1983. Springer Netherlands, Dordrecht, pp. 81–95.

Larionov, V.V., 1969. Borehole Radiometry. U.S.S.R., Moscow (Nedra).

Linjordet, A., Olsen, R.G., 1992. The jurassic snohvit gas field, Hammerfest Basin, offshore northern Norway. In: Halbouty, M.T. (Ed.), M54: Giant Oil and Gas Fields of the Decade 1978-1988. The American Association of Petroleum Geologists, pp. 349–370.

Maast, T.E., Jahren, J., 2013. Is grain-to-grain pressure solution contributing to quartz cementation in sandstones? In: Proceedings of the 75th EAGE Conference and Exhibition Incorporating SPE EUROPC, London. Earthdoc Th-09-11, pp. 1–4.

Maast, T.E., Jahren, J., Bjørlykke, K., 2011. Diagenetic controls on reservoir quality in

middle to upper jurassic sandstones in the south viking graben, north sea. AAPG Bull. 95, 1937–1958.
Magara, K., 1978. Compaction and Fluid Migration- Practical Petroleum Geology. Elsevier.
Marcussen, Ø., Maast, T.E., Mondol, N.H., Jahren, J., Bjørlykke, K., 2010. Changes in physical properties of a reservoir sandstone as a function of burial depth – the Etive Formation, northern North Sea. Mar. Petrol. Geol. 27, 1725–1735.
Mondol, N.H., Bjørlykke, K., Jahren, J., Høeg, K., 2007. Experimental mechanical compaction of clay mineral aggregates—changes in physical properties of mudstones during burial. Mar. Petrol. Geol. 24, 289–311.
Nooraiepour, M., Mondol, N.H., Hellevang, H., Bjørlykke, K., 2017. Experimental mechanical compaction of reconstituted shale and mudstone aggregates: investigation of petrophysical and acoustic properties of SW Barents Sea cap rock sequences. Mar. Petrol. Geol. 80, 265–292.
NPD, 2019. Norwegian Petroleum Directorate FactPages.
Nyland, B., Jensen, L.N., Skagen, J., Skarpnes, O., Vorren, T., 1992. Tertiary uplift and erosion in the Barents Sea: magnitude, timind and consequences. In: Larsen, R.M., Brekke, H., Larsen, B.T., Talleraas, E. (Eds.), Structural and Tectonic Modelling and its Application to Petroleum Geology. NPF Special Publication 1. Elsevier, Amsterdam, pp. 153–162.
Oelkers, E.H., Bjørkum, P.A., Murphy, W.M., 1992. The mechanism of porosity reduction, stylolite development and quartz cementation in North Sea sandstones. In: In: Kharaka, Y.K., Maest, A.S. (Eds.), Water-Rock Interaction: Rotterdam, Balkema, vol. 2. pp. 1183–1186.
Oelkers, E.H., Bjørkum, P.A., Murphy, W.M., 1996. A petrographic and computational investigation of quartz cementatioin and porosity reduction in North Sea sandstones. Am. J. Sci. 296, 420–452.
Ohm, S.E., Karlsen, D.A., Austin, T.J.F., 2008. Geochemically driven exploration models in uplifted areas: examples from the Norwegian Barents Sea. AAPG Bull. 92, 1191–1223.
Olaussen, S., Dalland, A., Gloppen, T.G., Johannessen, E., 1984. Depositional environment and diagenesis of Jurassic reservoir sandstones in the eastern part of Troms I area. In: Spencer, A.M. (Ed.), Petroleum Geology of the North European Margin: Proceedings of the North European Margin Symposium (NEMS '83), Organized by the Norwegian Petroleum Society and Held at the Norwegian Institute of Technology (NTH) in Trondheim 9–11 May, 1983. Springer Netherlands, Dordrecht, pp. 61–79.
Ødegaard, E., Avseth, P., 2003. Interpretation of Elastic Inversion Results Using Rock Physics Templates. EAGE, Expanded Abstracts.
Paxton, S.T., Szabo, J.O., Ajdukiewicz, J.M., Klimentidis, R.E., 2002. Construction of an intergranular volume compaction curve for evaluating and predicting compaction and porosity loss in rigid-grain sandstone reservoirs. AAPG Bull. 86, 2047–2067.
Peltonen, C., Marcussen, O., Bjørlykke, K., Jahren, J., 2008. Mineralogical control on mudstone compaction: a study of Late Cretaceous to Early Tertiary mudstones of the Vøring and Møre basins, Norwegian Sea. Petrol. Geosci. 14, 127–138.
Prasad, M., Meissner, R., 1992. Attenuation mechanisms in sands - laboratory versus theoretical (biot) data. Geophysics 57, 710–719.
Ramm, M., 1991. Porosity-depth Trends in Reservoir Sandstones: Diagenesis and Porosity Evolution of Lower and Middle Jurassic Reservoir Sandstones in the Troms I Area, Barents Sea. PhD Thesis, University of Oslo, Norway.
Ramm, M., 1992. Porosity depth trends in reservoir sandstones - theoretical-models related to Jurassic sandstones Offshore Norway. Mar. Petrol. Geol. 9, 553–567.
Ramm, M., Forsberg, A.W., Jahren, J.S., 1997. Porosity-depth trends in deeply buried upper jurassic reservoirs in the Norwegian central graben: an example of porosity preservation beneath the normal economic basement by grain-coating microquartz. In: In: Kupecz, J.A., Gluyas, J., Bloch, S. (Eds.), Reservoir Quality Prediction in Sandstones and Carbonates, vol. 69. AAPG Memoir, pp. 177–199.
Riis, F., Fjeldskaar, W., 1992. On the magnitude of the late tertiary and quaternary erosion and its significance for the uplift of scandinavia and the Barents Sea. In: In: Larsen, R.M., Brekke, H., Larsen, B.T., Talleraas, E. (Eds.), Structural and Tectonic Modcelling and its Application to Petroleum Geology. Elsevier, Amsterdam, vol. 1. NPF Special Publication, pp. 163–185.
Rittenhouse, G., 1971. Pore space reduction by solution and cementation. AAPG Bull. 55, 80–91.
Stone, W.N., Siever, R., 1996. Quantifying compaction, pressure solution and quartz cementation in moderately- and deeply-buried quartzose sandstones from the Greater Green River Basin, Wyoming. In: In: Crossey, L.J., Loucks, R., Totten, M.W. (Eds.), Siliciclastic Diagenesis and Fluid Flow, vol. 55. Society for Sedimentary Geology Special Publications, pp. 129–150.
Storvoll, V., Bjørlykke, K., Mondol, N.H., 2005. Velocity-depth trends in mesozoic and cenozoic sediments from the Norwegian shelf. AAPG Bull. 89, 359–381.
Storvoll, V., Brevik, I., 2008. Identifying time, temperature, and mineralogical effects on chemical compaction in shales by rock physics relations. Lead. Edge 27, 750–756.
Tada, R., Siever, R., 1989. Pressure solution during diagenesis. Annu. Rev. Earth Planet Sci. 17, 89–118.
Thyberg, B., Jahren, J., 2011. Quartz cementation in mudstones: sheet-like quartz cement from clay mineral reactions during burial. Petrol. Geosci. 17, 53–63.
Vernik, L., Nur, A., 1992. Petrophysical classification of siliciclastics for lithology and porosity prediction from seismic velocities. AAPG Bull. 76, 1295–1309.
Walderhaug, O., 1994. Precipitation rates for quartz cement in sandstones determined by fluid-inclusion microthermometry and temperature-history modeling. J. Sediment. Res. B Stratigr. Global Stud. 64, 324–333.
Walderhaug, O., 1996. Kinetic modeling of quartz cementation and porosity loss in deeply buried sandstone reservoirs. AAPG Bull. 80, 731–745.
Walderhaug, O., Bjørkum, P.A., 2003. The effect of stylolite spacing on quartz cementation in the Lower Jurassic Sto Formation, southern Barents Sea. J. Sediment. Res. 73, 146–156.
Walderhaug, O., Oelkers, E.H., Bjorkum, P.A., 2004. An analysis of the roles of stress, temperature, and pH in chemical compaction of sandstones-discussion. J. Sediment. Res. 74, 447–449.
Waples, D.W., Couples, G.D., 1998. Some thoughts on porosity reduction — rock mechanics, overpressure and fluid flow. Geological Society, London, Special Publications 141, 73–81.
Worden, R.H., Morad, S., 1999. Clay minerals in sandstones: controls on formation, distribution and evolution. In: Worden, R.H., Morad, S. (Eds.), Clay Mineral Cements in Sandstones. Blackwell Publishing Ltd., Oxford, UK. https://doi.org/10.1002/9781444304336.ch1.
Zadeh, M.K., Mondol, N.H., Jahren, J., 2016. Experimental mechanical compaction of sands and sand–clay mixtures: a study to investigate evolution of rock properties with full control on mineralogy and rock texture. Geophys. Prospect. 64, 915–941.
Zimmer, M., Prasad, M., Mavko, G., 2002. Pressure and porosity influences on VP − VS ratio in unconsolidated sands. Lead. Edge 21, 178–183.
Zimmer, M.A., Prasad, M., Mavko, G., Nur, A., 2007. Seismic velocities of unconsolidated sands: Part 2 - influence of sorting- and compaction-induced porosity variation. Geophysics 72, E15–E25.